PLOS GENETICS

Allele surfing causes maladaptation in a Pacific salmon of conservation concern

Quentin Rougemont[1]*, **Thibault Leroy**[2], **Eric B. Rondeau**[3], **Ben Koop**[4], **Louis Bernatchez**[5]

1 Centre d'Ecologie Fonctionnelle et Evolutive, Univ Montpellier, CNRS, EPHE, IRD, Montpellier, France, **2** GenPhySE, INRAE, INP, ENVT, Université de Toulouse, Auzeville- Tolosane, France, **3** Department of Fisheries and Ocean, Pacific Biological Station, Nanaimo, Canada, **4** Department of Biology, University of Victoria, Victoria, Canada, **5** Département de Biologie, Institut de Biologie Intégrative et des Systèmes (IBIS), Université Laval, Québec, Canada

* quentinrougemont@orange.fr

Abstract

How various factors, including demography, recombination or genome duplication, may impact the efficacy of natural selection and the burden of deleterious mutations, is a central question in evolutionary biology and genetics. In this study, we show that key evolutionary processes, including variations in i) effective population size (N_e) ii) recombination rates and iii) chromosome inheritance, have influenced the genetic load and efficacy of selection in Coho salmon (*Oncorhynchus kisutch*), a widely distributed salmonid species on the west coast of North America. Using whole genome resequencing data from 14 populations at different migratory distances from their southern glacial refugium, we found evidence supporting gene surfing, wherein reduced N_e at the postglacial recolonization front, leads to a decrease in the efficacy of selection and a surf of deleterious alleles in the northernmost populations. Furthermore, our results indicate that recombination rates play a prime role in shaping the load along the genome. Additionally, we identified variation in polyploidy as a contributing factor to within-genome variation of the load. Overall, our results align remarkably well with expectations under the nearly neutral theory of molecular evolution. We discuss the fundamental and applied implications of these findings for evolutionary and conservation genomics.

Author summary

Understanding how historical processes, such as past glaciations, may have impacted variations in population size and genetic diversity along the genome is a fundamental question in evolution. In this study, we investigated how recent postglacial demographic expansion has affected the distribution of deleterious genetic variants and the resulting deleterious mutation load in Coho salmon (*Oncorhynchus kisutch*), throughout its native range in North America. By sequencing the entire genome of 71 Coho salmon, we reveal that postglacial expansion has led to allele surfing, a process where alleles increase in frequency in populations that are expanding or colonizing new environments. Here, allele

surfing resulted in an increased deleterious mutation load at the colonization front. Furthermore, we demonstrated that the efficacy of natural selection scales with variation in effective population size among populations. We showed that the specific genomic features of Coho salmon, namely variation in local recombination rate and variation in chromosomal inheritance, strongly impacted the segregation of deleterious mutations.

Introduction

Demographic events, including population contractions, expansions and secondary contacts have profound impacts on the spatial distribution of genetic diversity within species [1]. Range expansions can be accompanied by multiple founder events when few individuals colonize new areas. At the wave front, this process results in increased genetic drift and a reduced effective population size [2, 3]. This has multiple consequences genome-wide including (i) extended linkage disequilibrium [4], (ii) a loss of genetic diversity and (iii) increased levels of genetic differentiation [2, 3, 5]. At the wavefront, increased genetic drift favors allele surfing, a process that will increase the relative proportion of neutral, deleterious or advantageous mutations that will fix in the population [5–7]. Such allele surfing is expected to have two main negative consequences at the wave front: *i*) an increase of the deleterious load (called expansion load [8, 9]) and *ii*) a loss of adaptive potential [10].

First, allele surfing through increased genetic drift can overwhelm the effect of weak purifying selection, resulting in an increase of the deleterious load [11]. Due to the lower efficacy of natural selection in low N_e populations, a greater fraction of slightly deleterious mutations is expected to be present in populations at the wavefront (*i.e.*, elevated ratios of non-synonymous to synonymous nucleotide diversity (π_N/π_S) [8, 9]). Moreover, under the nearly neutral theory of molecular evolution, the reduced efficacy of purifying selection in small populations should increase the fixation rate of slightly deleterious mutations [12]. On the other hand, given that most deleterious mutations are expected to be recessive, increased homozygosity of deleterious mutations should enable their removal more efficiently through genetic purging, leading to a reduction of the recessive and additive load [13]. To take this into account, a possible strategy is to investigate both the additive (i.*e*,. total) and the recessive (*i.e.*, fixed) deleterious mutation load. [8]. Evidence for an increased recessive genetic load has been reported in humans which has been associated with the Out-of-Africa bottleneck [14, 15]. Evidence has also been gathered in expanding populations in plants [16–20]. For instance in *Arabidopsis lyrata*, range expansion has been associated with an increased mutational load [16] and increased linkage disequilibrium [21]. Similar results were observed in *Escherichia coli [22]*. In contrast, a recent study in *A. lyrata* found no evidence of increased load following range expansion [23].

Second, allele surfing is expected to lead to a loss of adaptive potential due to a reduction in the rate of adaptive substitutions given that the supply of new mutations is proportional to N_e *[24]*. Unless compensatory mutations (*i.e.*, favourable mutations whose probability of occurrence increases to compensate for the fixation of slightly detrimental mutations–themselves with a higher probability of fixation in small populations–), counteract this effect in populations with a low N_e [25], one expects a lower proportion of substitutions driven by positive selection [26]. Support for a decreased rate of adaptation associated with range expansion was documented, particularly in plants [17, 20]. For instance, such a pattern was reported in the North American populations of *A. lyrata[17] [27]*, but not in the European ones despite a slight increase in their genomic burden [23]. Similarly an increased load is observed in human populations, a result that matches theoretical expectations under the out-of-Africa scenario

[28] but with limited evidence of a decrease in the efficacy of natural selection [29]. Beyond application to plants, humans and bacteria, there is a lack of empirical studies documenting the consequences of range expansion on the deleterious mutation load and the efficacy of natural selection.

Geographic variation in the overall mutation load is not the only interesting pattern to investigate; the genomic scale is also important. Both deleterious load and efficacy of selection are expected to vary along the genome depending on the local recombination rate [30, 31]. Non-recombining regions are expected to more freely accumulate deleterious mutations, a process called Muller's Ratchet [32]. Moreover, Hill-Robertson interference, a process whereby competing alleles interfere with each other to become fixed, increases the fixation rate of deleterious variants linked to positively selected sites. Such a process will be exacerbated in the absence of recombination [30, 33].

In species that have undergone a whole-genome duplication (WGD) with associated residual polyploidy, variation in chromosomal inheritance and genomic architecture may affect the distribution of deleterious mutations along the genome [34]. By doubling the chromosome number, WGD has major consequences. In the short term, WGD alters gene expression and favours polyploid dysfunction (reviewed in [35]). In the middle to long-term, the progressive return to a diploid state will result in regions of residual tetraploidy. Such regions should display an increased effective population size as compared to the rest of the genome ($4 N_e$ instead of $2 N_e$) and therefore a higher efficacy of selection and a reduced genetic load. Similarly, the population scale recombination rate, which also depends on N_e, should favour a higher efficacy of selection and a reduced genetic load. We thus predict that these regions should display a lower genetic load compared to diploid regions of the genome [36]. WGD has been associated with a reduced efficacy of purifying selection which may favour the accumulation of transposable elements. Such WGD may in turn have contrasted effects, as observed in plants [37, 38]. For instance, a LTR insertion favouring early flowering time (an adaptive trait in harsh environments), was shown to be present in tetraploid populations, but not in diploid populations of *A. arenosa*. In contrast, WGS was shown to be associated with small but significant differences in the load and distribution of fitness effect in the same species.

The Coho salmon (*Oncorhynchus kisutch*) is a Pacific salmon species of major cultural and economical importance, which has severely declined over the last decades (reviewed in [39]). It has undergone further recent declines in multiple parts of its native range [40]. In addition to human-induced perturbations, the species has undergone a series of postglacial expansions from its main glacial refugium (Cascadia/California) with multiple founder events along its route toward Alaska, leading to a pattern of isolation by distance, a gradient of population structure and a decrease in genetic diversity [41–43]. Accordingly, these range expansions may result in an increased expansion load, questioning whether such load may have consequences on the fitness of populations at the expansion front. The Coho salmon offers a unique opportunity to test the role of demography and recombination on the deleterious load and on the efficacy of selection. The Coho salmon belongs to the Salmonidae family, a particularly relevant group of species to investigate the effect of WGD. The common ancestor of all present-day salmonids has undergone a whole-genome duplication event ~80-100MyA [44]. The genome of salmonid species is still on its path to rediploidization. For instance, approximately 8% of the Coho salmon genome displays residual tetraploidy [41]. Residual tetraploidy offers a unique opportunity to investigate the direct effect of the genomic variation of N_e on the efficacy of selection.

To address these questions, we aimed at testing the following general hypotheses: i) whether demographic expansion and bottlenecks have led to an increased load and decreased efficacy of selection, ii) whether heterogeneous recombination levels shape the within-genome

variation of the load as a result of Hill-Robertson effects and iii) whether residual tetraploidy results in an increased efficacy of selection and reduced deleterious load through increased recombination and N_e.

Results and discussion

Strong postglacial population expansion revealed through whole genome sequences

We generated 30X coverage whole genome resequencing data for 71 Coho salmon representing 14 populations distributed from California to some of the most upstream populations of the Porcupine River in Yukon, Canada (**Fig 1A**). We also included several outgroup species namely the Sockeye salmon (*O. nerka*), Chinook salmon (*O. tshawytscha*), Pink salmon *(O. Gorbuscha)*, Rainbow trout (*O. mykiss*) and Atlantic salmon (*Salmo salar*). These genomes were used to identify the ancestral and derived alleles in Coho and/or testing correlation(s) between genomic load estimates and recombination rate (**S1–S3 Tables**).

To explore the amount of clustering among individuals a PCA was performed (**S1A and S1B Fig**). The PCA illustrates that populations are spatially structured following both latitudinal and longitudinal gradients. The first axis strongly correlates with both latitude (Pearson r = 0.97, p < $2e^{-16}$) and longitude (Pearson r = -0.82, p < $2e^{-16}$), as expected when space drives population structure [45]. Moreover, admixture analyses (**S1B Fig**) revealed that Coho populations were generally structured at the river/watershed level. These observations corroborate our previous inferences based on lower resolution genomic dataset [42, 43].

Under a single refugial expansion scenario, we expect a linear decrease in genetic diversity as a function of the distance from the source. We plotted the distribution of observed heterozygosity (H_o) as a function of the distance to the southernmost sample and observed a negative correlation with the distance to the southernmost site (R^2 = 0.77, p<$2e^{-16}$, **S2B Fig**). Next, we
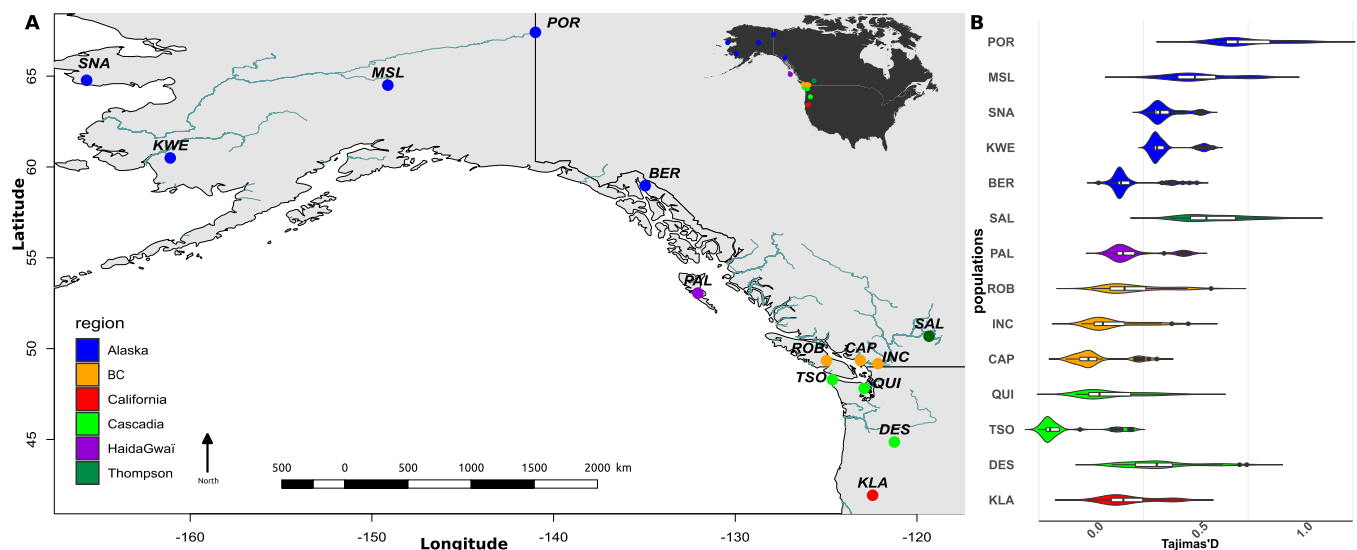
Fig 1. Sampling design and population size change inferred through whole genome sequences. A) Sample site along the Pacific coast of North America. Map produced in R using the World data from Maps package with public domain data available at [47]. B) Average Tajima's D values computed along the genome and summarized for each sample locality. Populations are ordered from distance to the river mouth and from the South to the North (i) California, (ii) Cascadia, (iii) British-Columbia (BC), (iv) Haida-Gwaii, (v) Salmon River (Fraser Basin) and (vi) Alaska. Abbreviation provided in S2 Table). Tajima's D values vary positively as a function of the distance from the southernmost site (R^2 = 0.28, p <$2e^{-16}$) and as a function of the distance to the river mouth (R^2 = 0.47, p <$2e^{-16}$) reflecting the history of founder events from downstream to upstream sites.

https://doi.org/10.1371/journal.pgen.1010918.g001

used the β_{ST} coefficient to identify the most likely ancestral populations from which the expansion could have started. β_{ST} can account for the non-independence among populations and negative values are indicative of ancestral populations [46]. This metric was also positively correlated with distance to the southernmost site ($R^2 = 0.75$, $p < 2e^{-16}$, **S2A Fig**).

The Salmon River population from the Thompson area (dark green point, **Figs 1A** and **S2A**) exhibits lower diversity levels, as compared to all non-Alaskan populations. Excluding this outlier river, revealed even stronger correlations, with a correlation with β_{ST} and H_O respectively raising to $R^2 = 0.88$ and $R^2 = 0.90$ ($p < 2e^{-16}$ for both tests), suggesting an overall clear spatial pattern across the populations sampled, with the notable exception of this specific population which had a different demographic trajectory in this population, which seems consistent with a strong bottleneck and inbreeding [41].

Another indicator of changes in population sizes is an increase in Tajima's D values at the genome-wide level. We tested the hypothesis of increased Tajima's D values as a function of (i) the traveled distance from the southernmost site (reflecting northward postglacial expansion) and (ii) the distance to the sea only (reflecting upstream directed founder events). Results are consistent with a signal of population expansion along the colonization axis from the south to the north based on Tajima's D values ($R^2 = 0.28$, $p < 2e^{-16}$, **Fig 1B**). Distance to the sea is also highly significant ($R^2 = 0.47$, $p < 2e^{-16}$ for Tajima's D). This suggests that more genetic drift occurs in upstream populations e.g. Porcupine (POR), Mile Slough (MSL), Thompson (SAL) and Deschutes (DES).

Another hallmark of population bottlenecks and genetic drift associated with founder events is an increase in linkage disequilibrium across the genome [4]. We tested this hypothesis by measuring linkage disequilibrium (r^2) following Hill & Robertson [48]. In line with the above observations, we observed extended linkage disequilibrium (LD) along the genome in remote Alaskan/Yukon populations (Porcupine and Mile Slough Rivers) and in the Salmon R. population (Thompson R. Watershed, **S2C Fig**). Accordingly, the LD decay—here defined as a r^2 reaching half of its maximum value—is observed at 25, 12 and 6 kbp in these three populations, contrasting with values around 0.5 kbp observed in the other populations(**S2C Fig**). These results show a large among population variance in effective population sizes, likely associated with the strength of the founder events.

In addition, we constructed a population phylogeny based on a matrix of pairwise F_{ST} values computed between each pair of populations (**Fig 2A and 2B**) and on a matrix of variance-covariance in allele frequencies implemented in Treemix [49] (**S3 Fig**). Both analyses confirmed that populations located in the north underwent more genetic drift, in line with the postglacial expansion from the south to the north and the subsequent founder effects associated with upstream colonisation of the rivers from the west to the east.

To consolidate the above observations, we investigated historical changes in N_e using the Sequentially Markovian Coalescent in SMC++ [50]. This method takes advantage of both the SMC and of the site frequency spectrum to infer change of effective population size though time. We inferred such changed for each population separately (**S2D Fig**), testing a mutation rate of $8e^{-9}$ and $1.25e^{-8}$ mutations/bp/generation, which respectively corresponds to the median and the mean mutation rate estimated in Atlantic salmon (*salmo* salar), a closely related salmonid (J. Wang, personal communication). This analysis revealed: *i)* an expansion of most populations approximately 12–20 KyA ago, concomitant with postglacial recolonization, *ii)* a slow and steady demographic decline in the Thompson R. (**S2D Fig**), and *iii)* a split time between all pairwise combinations of populations (median = 16,3 KyA, range = 6,7KyA - 61KyA, **S4 Fig**) compatible with the onset of postglacial population expansion and colonisation of different rivers following glacial retreat [41, 42]. Using the mean mutation rate yielded similar results with a more recent estimates of split times (median = 9,6 KyA, **S4 Fig**) (min = 5
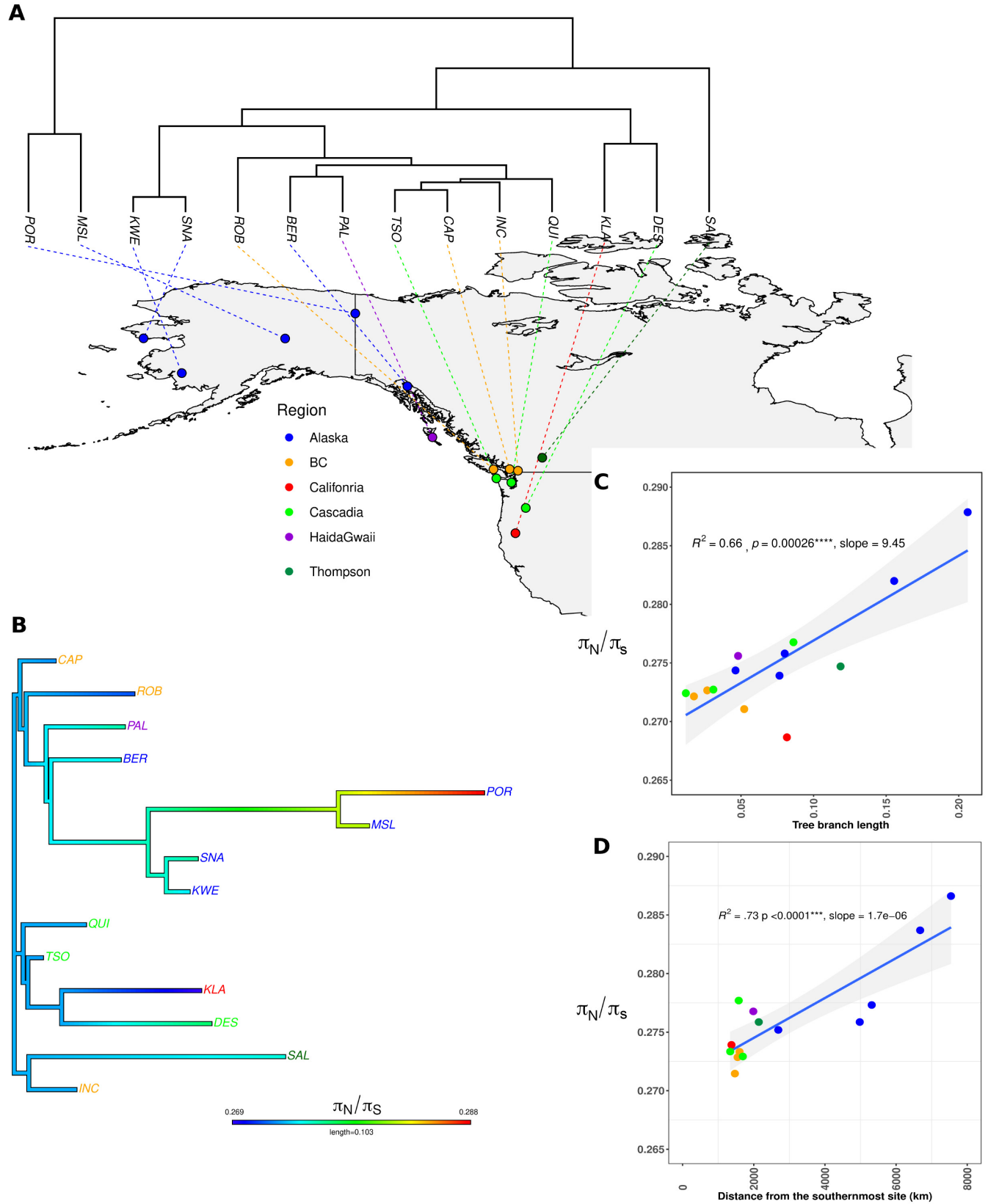
Fig 2. Expansion routes inferred from phylogenetic analyses revealed the extent of the mutation load. A) population phylogenetic tree inferred from the pairwise F_{ST} values (see also S3 Fig) superimposed on the map. Map produced with R using the worldHires data [51]. B) Population specific branches are coloured according to the π_N/π_S values, used as a proxy of the genetic load. C) Correlation between tree branch lengths to the root and the π_N/π_S ratio. D) Correlation between the travelled distance to the southernmost site and the π_N/π_S ratio. The blue line represents the slope of the linear model between the two variables. The grey area in panel C and D represents the 95% confidence interval levels around the regression lines.

KyA–max = 18 KyA). Overall, SMC++ results indicate that all populations shared a similar demographic history until they began to diverge following the end of the last glacial cycle (see **S1 Note** and associated Supplementary Tables).

Range expansion explained variation in the mutation load

We estimated the mutation load of the populations using different metrics: *i)* π_N/π_S, *ii)* count of derived homozygous mutations (including both missense and Loss-of-function (LoF) mutations), and *iii)* total count of derived mutations (including both missense and LoF mutations). We observed a significant positive correlation of the π_N/π_S ratio of each local population and the distance to the southernmost site (see methods), corresponding to the most-likely refugia as discussed in our previous work [42] (R^2 = 0.73, p<0.0001, **Fig 2D**). Similarly, using the tree branch length to the root of our tree (**Fig 2B**) as a proxy of expansion route revealed a significant correlation with the π_N/π_S ratio (R^2 = 0.66, p<0.0001, F**ig 2C**). This result was also supported by an analysis considering tree branch lengths inferred with Treemix (**S4 Table**). Accordingly, there was a significant correlation between π_N/π_S and two different proxies of the effective population size, namely levels of nucleotide diversity at synonymous sites (π_S) and SMC++ N_e, expected to be reduced at the colonization front and in bottlenecked populations (π_S in **S5A Fig** and SMC++ N_e in **S5B Fig**). These results support expectations pertaining to variation in mutation load under a model of expansion load (e.g. [28]).

The interpretation of π_N/π_S in populations that are not at mutation-drift equilibrium (say after a bottleneck) is however difficult, since π_N will reach an equilibrium value faster than π_S because selected alleles will be subject to higher negative selection and undergo a faster turnover [14, 52, 53]. Thus, the π_N/π_S may not be the best predictor of the total burden of deleterious mutations, as it is potentially affected by demography and selection [14]. To circumvent this limitation, we counted and plotted the distribution of non-synonymous mutations classified according to i) their impact and expected consequences on fitness (*i.e.* missense and LoF mutations) and; ii) segregation patterns (*i.e.* additive (total) load composed of heterozygous and derived homozygous genotypes or recessive (fixed) load composed of homozygous derived genotype) [54]. Just as the π_N/π_S, we found a significant association between the derived load and the distance to the southernmost sites both for missense mutations (R^2 = 0.790, p < 0.001, **Fig 3A**) and for LoF mutations (R^2 = 0.777, p < 0.001, **Fig 3B**). Similarly, we observed a significant association between the tree branch length to the root and the derived load of missense and LoF mutations (R^2 = 0.39, p = 0.0096 and R^2 = 0.40, p = 0.009, respectively, **S4 Table**).

The most deleterious mutations are efficiently purged across the range

The total number of missense mutations was significantly more abundant in the more southern populations (*i.e* California, Cascadia, **S5 Table** for all Tukey-HSD *p-values*) than in northern ones (**Fig 3A**), while it was nearly constant from the south to the north regarding LoF mutations (**Fig 3B**), with no significant differences among populations (**S5 Table**). The southernmost populations displayed a higher load of mutations in heterozygous state (**Fig 3**), as expected due to their higher historical effective population size, favouring the segregation of recessive mutations hidden in a heterozygous state [42, 55].
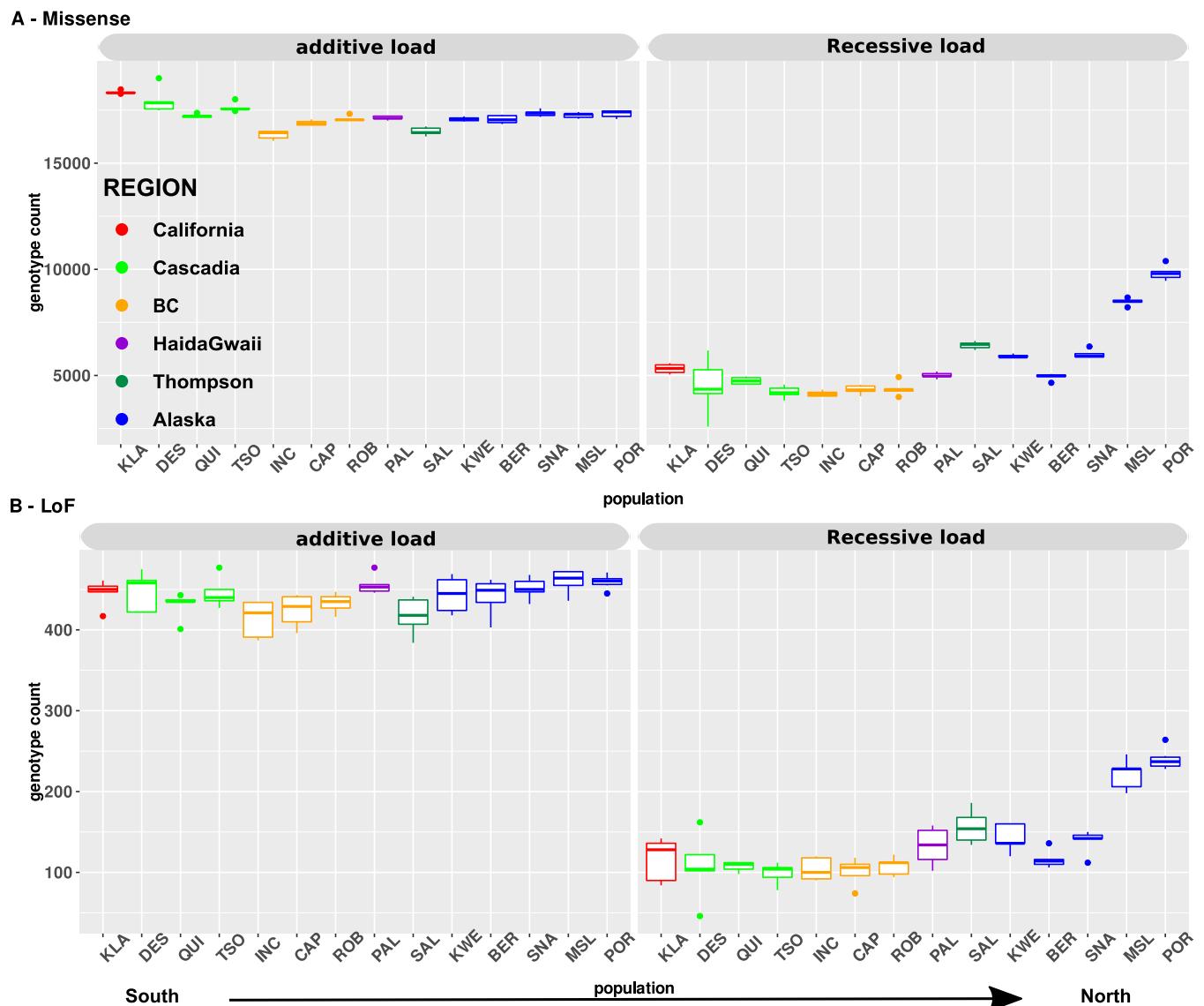
Fig 3. Number of deleterious alleles per riverper individual for all populations sorted from the South to the North. *The plot* shows the additive load (left panel) and recessive derived homozygous load (right panel) for A) missense mutations and B) Loss-Of-Function (LoF) mutations. No strong differences are observed in the additive load among populations. In contrast, significant differences were observed for the recessive load in populations at the expansion front both for missense mutations and LoF mutations and this was significantly correlated with the distance to the southernmost site. Each color represents a major regional group. Abbreviation for each site is provided in S1 Table.

https://doi.org/10.1371/journal.pgen.1010918.g003

The fixed load increases with population expansion

The fixed load (i.e. count of derived homozygous sites) increased from south to north for both missense and LoF with the most extremes samples, including Mile Slough (MSL), Porcupine (POR) and Salmon (SAL) rivers being the most significantly loaded (**S5 Table**), as expected due to founder events and allele surfing for Alaskan/Yukon samples and due to bottlenecks for the Salmon River (**Fig 3** right panel).

Range expansion have reduced the efficacy of selection at range margin

We predicted that selection efficacy will be reduced at the expansion front and in populations with a lower N_e. To test this, we measured three parameters, namely the rate of non-adaptive

and adaptive amino-acid substitutions relative to neutral divergence (ω_{NA} and ω_A, respectively; with $\omega_A = d_N/d_S - \omega_{NA}$) and the proportion of non-synonymous amino-acid substitution that result from positive selection ($\alpha = \omega_A/(d_N/d_S)$) using the software Grapes [56] using maximum likelihood estimation under a population genetic model. A general expectation is that populations at the expansion margin will exhibit a higher rate of non-adaptive substitutions (ω_{NA}), a lower rate of adaptive substitutions (ω_A) and a lower proportion of amino-acid substitutions (α).

We observed a reduced efficacy of purifying selection likely associated with the multiple founder events and bottlenecks which resulted in a decrease rate of adaptive substitutions (ω_A, $R^2 = 0.37$, $p = 0.013$) and increased ω_{NA} as a function of the distance to the South ($R^2 = 0.57$, $p = 0.0011$, **Fig 4A**). We also found a significant positive correlation between ω_{NA} and the distance to the ocean ($R^2 = 0.52$, $p = 0.002$, **S6A Fig**) and conversely a negative correlation between ω_A and the distance to the ocean ($R^2 = 0.40$, $p = 0.00895$, **S6B Fig**), suggesting that upstream populations displays a lower adaptive potential. This observation thus suggests that the population expansion had impacts on both the adaptive and non-adaptive substitution rates.

Similarly strong correlations were observed when considering the tree branch length to the root (details in **S7** and **S8** **Figs and S4 Table**). The Salmon R. population (Thompson R. watershed), which suffered a recent decline in abundance, supposedly due to the sustained release of hatchery fish derived from few individuals and the Ryman-Laikre effect [57] (see discussion below), also displayed a high ω_{NA}.

We also predicted a higher α value in populations with higher N_e and, conversely, a decreased value of α in populations with lower N_e. We observed a strong positive correlation between α and the synonymous nucleotide diversity (π_S) of each local population, which represents a good predictor of the long term (coalescent) N_e ($R^2 = 0.63$, $p = 0.0004$, **S9 Fig**). To more directly test the association with N_e, we correlated SMC++ based estimates of N_e (averaged over a 200KyA window) with α and recovered significant correlations ($R^2 = 0.49$, $p = 0.004$, **Fig 4B**). It is noteworthy that a good correlation between proxies of N_e obtained from SMC++ and π_S was also observed ($R^2 = 0.68$, $p = 0.00017$, results not shown). Altogether, the above results provide empirical support pertaining to the evolutionary consequences of
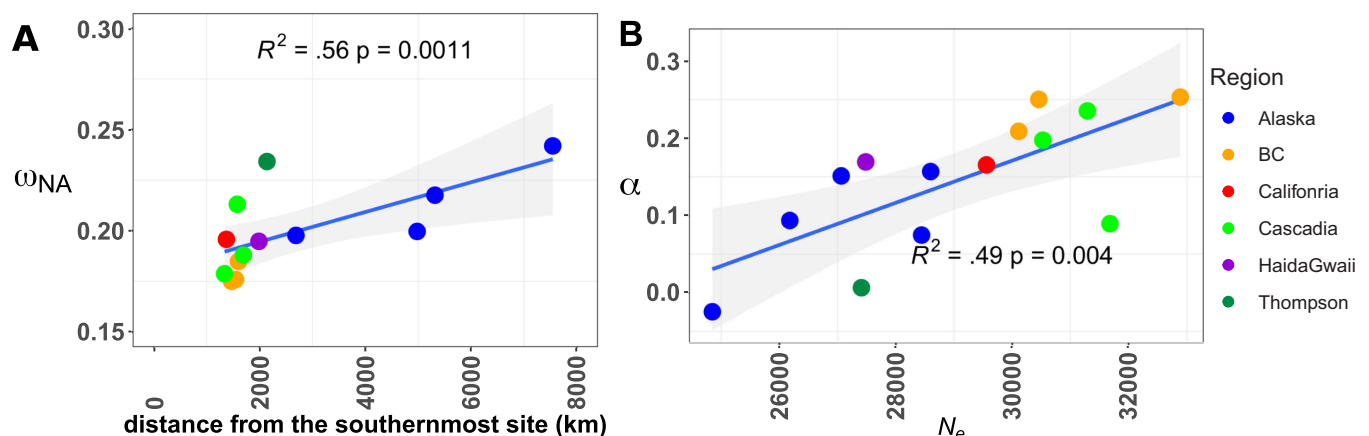
Fig 4. Efficacy of selection decreases at the expansion front and as a function of long-term effective population size. A) increased rate of nonsynonymous non-adaptive substitutions (ω_{NA}) in northernmost populations of Coho salmon (Alaska) and in the bottlenecked Thompson River. B) Correlation between α and historical variation in the coalescent effective population size estimated from SMC++. See also **S7** and **S8** **Figs** for correlations based on tree branch lengths. Note that the distance from the southernmost site was computed considering a Californian sample, from a previous study [42], for which no WGS data were available.

allele surfing at expanding range margins, in particular regarding the loss of adaptive potential and the mutation burden.

Recombination rates shape the deleterious mutational landscape

In addition to the spatial structure associated with the postglacial recolonization, we investigated the genome-wide variation in mutation load. Such variation could be associated with the occurrence of structural variants (e.g. chromosomal inversions) which may incur a significant load because deleterious recessive mutations may freely accumulate in the absence of recombination, as observed for instance in sex chromosome and related supergene-like architecture [58]. To test this hypothesis, we used the GC content at third codon position (GC3 hereafter) as a proxy of the rate of recombination [59, 60] (see S2 Note for an explanation). We observed strong correlations between levels of GC3 and π_N/π_S ratio for all Coho salmon populations (R^2 range = 0.938–0.955, p<0.001) except for population MSL (R^2 = 0.252; p = 0.0038) (Fig 5A). An analysis focused on GC-conservative sites, which are not affected by GC-biased Gene Conversion (gBGC), revealed similarly strong patterns across all Coho salmon populations (Fig 5B, R^2 range = 0.665–0.876, p < 0.01). π_N/π_S ratios estimated based on all sites or GC-conservative-sites only are highly correlated (Pearson r = 0.909, p <0.001). We tested the generality of this relationship using four other closely related Pacific salmon species and found strikingly similar pattern in Chinook salmon (R^2 GC3 ~ π_N/π_S = 0.9338, p = 1e-11) Sockeye and Kokanee salmon (R^2 range = 0.81–0.96, p <0.001), as well as Rainbow trout populations (R^2 range = 0.95–0.96, p <0.001, Fig 5C).

We then analyzed the difference in the correlations between levels of GC3 and π_N/π_S ratio among all Coho salmon populations. Indeed, the intensity of this correlation highlights the effect of recombination rate variation on the efficiency of purifying selection [61]. The populations at the expansion front (Mile Slough R., Porcupine R., Snake R.) in Alaska exhibit the lowest correlations between GC3 and π_N/π_S. If both demographic factors (*i.e.* distance to the source here) and genomic factors (*i.e.* recombination) interact to shape the load, we may
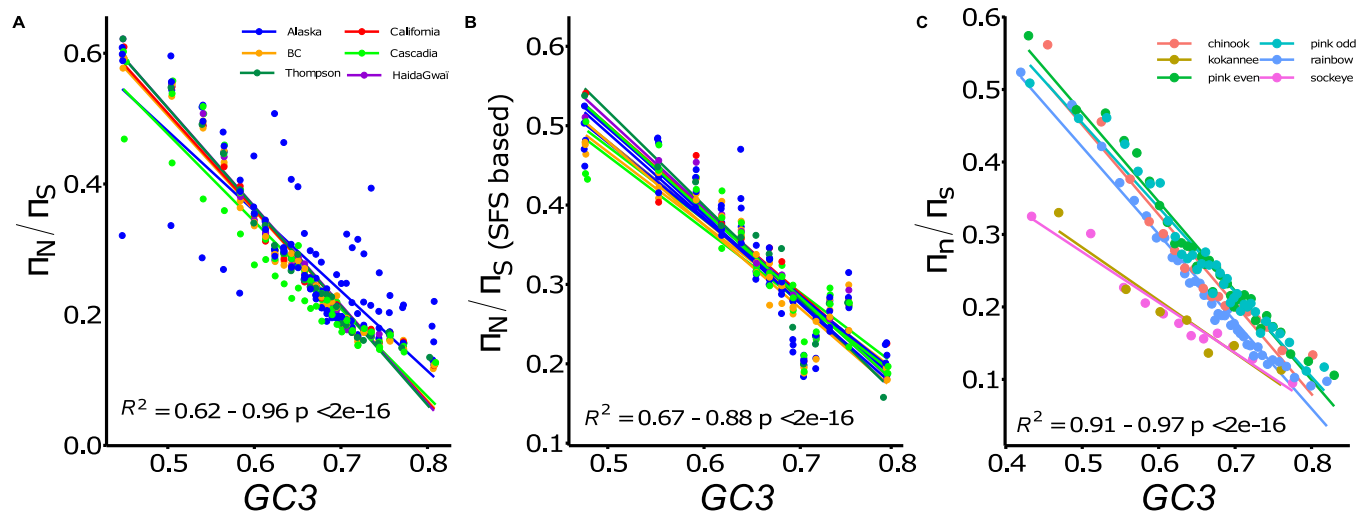
Fig 5. The deleterious load is determined by variation in GC3 content in multiple salmonids.) A) Correlations between the deleterious load (π_N/π_S) and GC content at third codon position in multiple Coho salmon populations. Each line represents the values colored by major regional groups (See S10A Fig for detail). B) Correlations between the deleterious load (π_N/π_S) and the GC content at third codon position considering an independent method based on the site frequency spectrum at GC-conservative sites. C) Correlation between the deleterious load (π_N/π_S) and GC content at third codon position in sockeye salmon ecotypes (sockeye and kokanee), chinook, pink salmon and in rainbow trout. Averages are provided for rainbow trout, salmon and kokanee at the species level, see S10B and S10C Fig for detail by population.

https://doi.org/10.1371/journal.pgen.1010918.g005

predict a positive relationship between these two factors because the northernmost populations should have an even higher load in regions of low recombination. We tested this hypothesis using a linear model between the slope of the regression between π_N/π_S and GC3 and the distance to the ancestral source populations did not reveal such a relationship (p = 0.133, **S11 Fig**).

Regions of residual tetraploidy revealed drivers of the load in Coho salmon

We tested the hypothesis that regions with residual tetraploidy exhibit a reduced load due to increased efficacy of purifying selection due to higher population sizes ($4Ne$ rather $2Ne$). Contrary to this expectation, increased deleterious load was observed in regions of residual tetraploidy (3,700 genes) as compared to diploid regions (**Fig 6A**, red dotted line mean $\pi_N/\pi_S >$ 0.35, diploid region $\pi_N/\pi_S < 0.30$). Given that we also observed lower levels of recombination in regions with residual tetraploidy compared to re-diploidized genomic regions (**S12 Fig**, p < 0.0001, W Mann-Whitney = $3.04e^7$, see also **S13 Fig** and **S6 Table** for differences in recombination among populations), our results suggest that this higher π_N/π_S could be mostly due to lower recombination rates. Another expected genomic consequence of this lower recombination rate is a higher load of transposable elements [62]. When computing the relative length of TE, *i.e.* the length of TE corrected by the chromosome length (see methods), we found a significant enrichment of TE in the regions of residual tetraploidy as compared to diploid chromosomes (**Fig 6B**, p <0.0001, WMann-Whitney = $1.36e^{10}$). This tendency was also observed across the different TE categories (**S14 Fig**). To more directly test the N_e-effect hypothesis, we eliminated the effect of the recombination rate by comparing the load across similar bins of GC in diploid vs. tetraploid regions. The π_N/π_S was systematically higher in diploid regions than in the tetraploid ones after excluding the class with the lowest GC content (**Fig 6C** and **S7 Table**) indicating that the load was significantly higher in diploid compared to tetraploid regions, with the notable exception of regions with extremely reduced recombination. Therefore, it is still possible that increased efficacy of selection is at play in recombining regions of residual tetraploidy, following the hypothesis of higher effective size in these regions.

Conclusion

The role of genetic drift, recombination, selection and variation in inheritance in affecting the deleterious load and efficacy of natural selection is a central question with fundamental and applied consequences for biodiversity.

Using population genomics analyses, we investigated the evolutionary consequences of recent demographic events in Coho salmon. Our results supported gene surfing across North America [42]. Results also supported lower N_e at the northern range expansion front, which induced two main evolutionary consequences: a surf of slightly deleterious mutations and a putative reduction of the adaptive potential, as expected under the nearly neutral hypothesis of molecular evolution [12].

We further demonstrated that one population, the Salmon River (Thompson R. watershed) displayed an increased fixed load and decreased selection efficacy compared to southern populations. Previous studies showed that this population is genetically isolated from others [42, 43, 63] and displayed genomic footprints of a bottlenecked population such as long runs of homozygosity [41]. This population has been subjected to extensive hatchery enhancement (from a single population) to circumvent the decline of Coho salmon in the Thompson drainage [64]. From a theoretical standpoint, if a few captive individuals were used as parents for subsequent releases, then an increase in inbreeding and a reduction in effective population size are
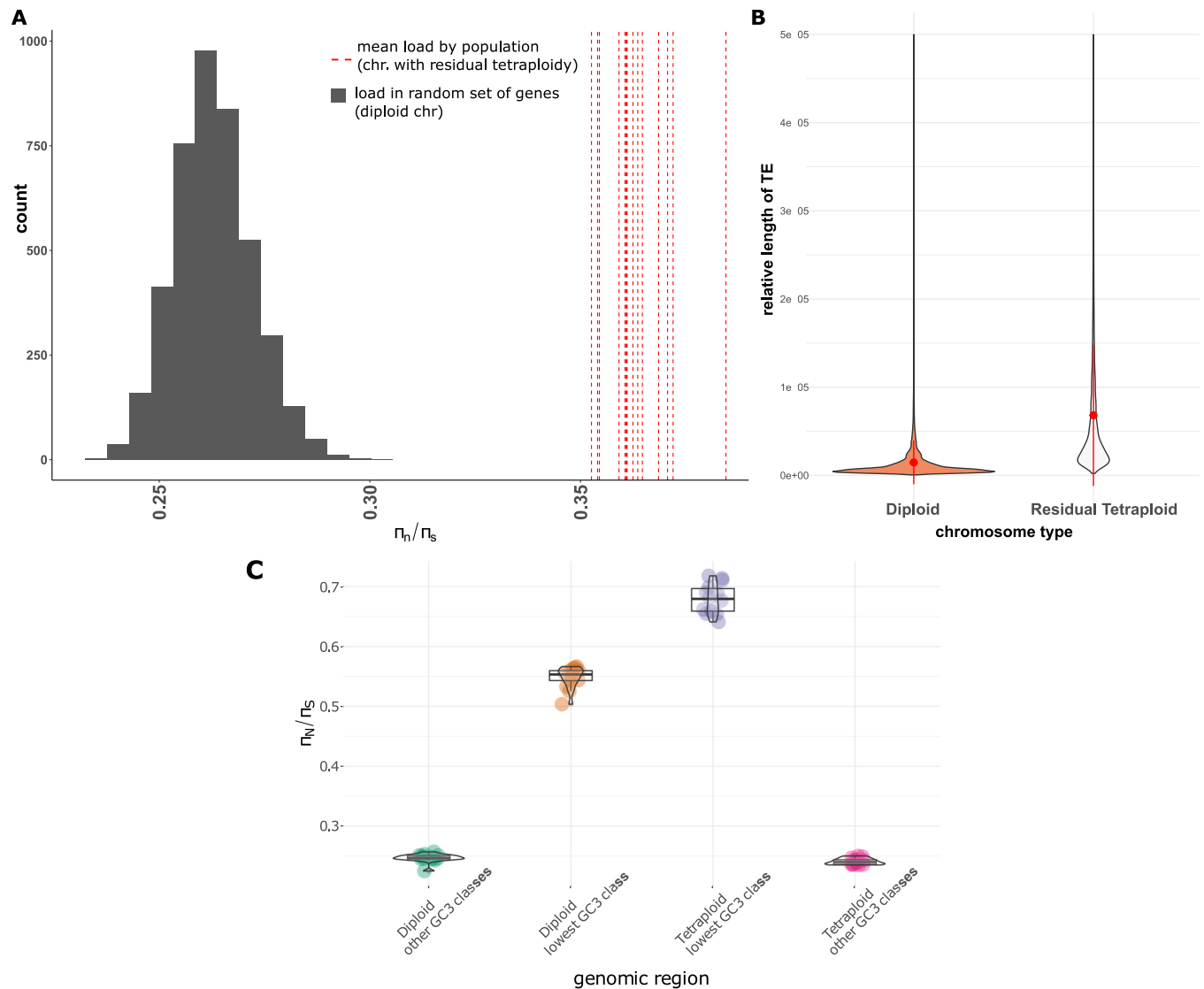
Fig 6. Increased load in region of residual tetraploidy. A) Distribution of π_N/π_S ratio when considering all genes in regions of residual tetraploidy (red lines) for each population compared to a set of 200 randomly generated samples of 4,000 genes in the rest of the genome (gray histogram). **B**) Violin plot showing that regions of residual tetraploidy displayed significantly longer transposable elements when compared to diploid regions. Orange = diploid chromosome. Gray = chromosome with residual tetraploidy. Red point = mean +/- 1*sd. **C**) Difference in the distribution of $\pi N/\pi S$ ratio in different genomic regions of the Coho salmon. Each dot represents the value observed for a given population in either diploid or tetraploid region with the "lowest" GC3 value (corresponding to low recombination) compared to the rest of GC3 values (labelle "other GC3", corresponding to intermediate to high recombination). The GC values were computed in 4mb windows separately for diploid and tetraploid regions.

https://doi.org/10.1371/journal.pgen.1010918.g006

expected, a phenomenon called the Ryman-Laikre effect [57] [65]. Consequently it is possible that the increased π_N/π_S, ω_{NA}, and fixed deleterious load could be explained by both long-term evolution at low N_e and by the Ryman-Laikre effect associated with hatchery enhancements. Regardless, this suggests that careful enhancement needs to be performed with a diversity of parents to maximize genetic diversity of supplemented populations. This result has implications for fisheries enhancement, as well as genetic rescue programs aiming at reducing the inbreeding load of declining populations and restoring the fitness of these populations.

It is noteworthy that the southernmost population (Klamath R, California) was not characterized by the highest α value. Several non-exclusive hypotheses may explain this pattern: first,

some Californian populations are known to have undergone strong recent (human-driven) decrease in abundance due to both habitat degradation and climate change, which may leave a detectable footprint in the genome [66]. The recent demography could have an impact on the accuracy of the fit of the synonymous and nonsynonymous SFS under Grapes. Second, the Klamath R. population is located in the far upstream part of that river, and may have undergone a founder event when reaching this upper part, a hypothesis that is supported by the correlations we observed between several metrics and distance to the river mouth. Finally, we did not include the southernmost populations from California, which are more likely to be more ancestral, as we previously reported [42].

Since the use of π_N/π_S ratio can be criticized [14, 67, 68], especially when used to quantify the load within species, we computed additional metrics [56] to more directly estimate mutation load, as advocated by others [14, 69]. In this case, we found small differences in the additive load among Coho salmon populations, but a linear increase in the recessive load as a function of the distance to the southernmost sites and as a function of the tree branch length, both are used as proxies of the expansion route.

We demonstrated that the π_N/π_S ratio was negatively correlated with the GC content at third codon position, which represents a good proxy of the local recombination rate (see **S2 Note**). The negative correlation between π_N/π_S and GC3 was repeatedly observed across different salmonid species using both a sequence based estimate of π_N/π_S and an estimate based on GC-conservative site (non-affected by gBGC) [60]. These results indicated that recombination plays a key role in explaining the variation in the mutation load along the genome in salmonids. Our study empirically supports theoretical work about the accumulation of slightly deleterious mutations in non-recombining regions [30, 32]. Similarly, increased prevalence of deleterious mutations in low recombining regions have been reported in plants [70] and in human populations [71–73]. In particular, recent work in human populations have shown that both variation in demographic history (i.e. change in effective population size) and recombination rates are affecting allele-specific expression of harmful mutations [71]. The authors showed that allele specific expression causes underexpression of harmful mutations more efficiently in normally and highly recombining regions compared to low recombining regions. They further documented variation of this process among populations with varying demographic histories.

In line with the key role of recombination rate, we observed that only regions of residual tetraploidy with extremely low recombination rate (lower GC content) displayed an increased load in Coho salmon, accumulating more transposable elements, suggesting efficient selection in more "normally" recombining region of residual tetraploidy. In particular, our results indicate that i) the regions of residual tetraploidy ($4N_e$) with a normal recombination rate do not display an increased load, which may be expected under the nearly neutral theory if higher N_e is associated with the efficacy of selection; ii) only region of extremely low recombination rate (lower GC content) displays the highest load, highlighting once again the primary role of recombination in shaping the load, with a higher contribution than N_e. A third factor is the variation in dominance of deleterious mutation. Indeed, a recent simulation study found that in the case of hard sweeps, dominance of recessive mutation was a central aspect determining the signal of sweeps in polyploid genomes [39]. A detailed investigation of this aspect in regions of residual tetraploidy was beyond the scope of our study but would be worthy of further investigation.

The detailed consequences of ongoing rediploidization have been extensively studied at the regulatory levels elsewhere, with support for an increased load (higher d_N/d_S and TE load) in duplicated genes undergoing lower expression [74]. Recent studies in polyploid plant species have also documented various evolutionary consequences of such duplication on local

variation in the load and efficacy of selection [35]. For instance in *A. arenosa*, a reduced efficacy of purifying selection was suggested in tetraploids (4X) genome compared to diploids (2X), and the authors suggest that this is because deleterious alleles are better masked in auto-tetraploids [38]. Similarly, a recent work in the allopolyploid cotton *(Gossypium)* demonstrated that this species accumulates more deleterious mutations than the diploid species [75]. This observation supports a theory proposed by Haldane that recessive deleterious mutations accumulate faster in allopolyploids because of the masking effect of duplicated genes [76]. To sum up, our results concur with predictions from the nearly neutral theory of molecular evolution [12], in which slightly deleterious mutations are effectively neutral and purged effectively in regions of higher recombination, except perhaps in populations at the extreme of the expansion front. Interestingly, these results indicate that regions of low-recombination re-diploidize later than other genomic regions. We are not aware of any paper having documented such patterns so far. Further studies of this process across more species would be welcome to validate the generality of this observation.

Finally, our results have implications for conservation practices. We showed that the additive load is approximately constant, indicative of efficient purging across populations for both missense and LoF, similar to some recent studies on several plant and animal models [77–80]. However, results indicate that population at higher latitude from the Yukon watershed (Mile Slough R., Porcupine R.) or from the bottlenecked Salmon R. have not entirely purged the most deleterious mutations, including missense and LoF mutations, which may impose a fitness cost to these populations. Further empirical evidence for a causal link between the putative fitness cost of LoF mutations and adaptive phenotypic variation will be necessary to validate our observations. With this caveat in mind, our results for the Salmon R could guide practices in supplementation programs. For instance, choosing a diversity of parents from moderately differentiated populations of modest size may help increase the levels of heterozygosity and mask the expression of recessive deleterious mutations [55]. This strategy could reduce the occurrence of deleterious alleles and counteract the Ryman-Laikre effect described above. Moreover, populations (e.g. most upstream Alaskan/Yukon populations) for which our results suggest a reduced adaptive potential are also the most strongly exposed to rapid climate change, as the rate of temperature increase is most rapid at higher latitudes [81]. In all cases, maximizing the connectivity among populations and limiting habitat degradation appears as fundamental strategies to maintain high effective population size and increase the adaptive potential of Coho salmon to the multiple ongoing anthropogenic pressures [82]. More generally, how best to manage declining populations and guide conservation policies in these conditions to minimize the load and/or maximize genetic diversity is another debated issue [55, 83–85]. In the meantime, while conservation genomics undoubtedly has a major role for the short-term preservation of endangered species, this should not override the crucial need for reducing human impacts on natural ecosystems to preserve biodiversity over long time scales [86].

Methods

Sampling design for Coho salmon

We sampled and sequenced 71 individuals representing 14 populations distributed from California to Alaska (**S1 Table**). A set of 55 individuals was sequenced on an Illumina HiSeq2500 platform [38] and the other 16 individuals were sequenced on a NovaSeq6000 S4 platform using paired-end 150 bp reads. Reads were processed using fastp for trimming [87], and mapped to the most recent Coho reference genome (https://www.ncbi.nlm.nih.gov/assembly/GCF_002021735.2/) using bwa mem v2 [88]. Reads with a minimum quality below 20 were

discarded with samtools v1.7. Duplicates were removed with picard (http://broadinstitute. github.io/picard/). SNP calling was performed using GATK v4.2 [89] using our pipeline available at github.com/quentinrougemont/gatk_haplotype/. We generated a Haplotype gVCF for each sample individually, combined all gVCF and then performed a joint genotyping. We checked the variants quality score of our data and filtered our genotypes according to their quality following GATK best practices and based on quantiles distributions of quality metrics. We excluded all sites that did not match the following criterion: MQ < 30, QD < 2, FS > 60, MQRankSum < -20, ReadPosRankSum < 10, ReadPosRankSum > 10. We also excluded multiallelic SNPs, as well as indels. Genotypes with a depth lower than 6 or higher than 100 reads were also excluded to remove low confidence genotypes potentially associated with paralogs. Finally, we also generated a separate vcf file using the—all-sites option to obtain a file with invariant position to reconstruct sequence data (see the **Genetic load estimation in Coho salmon and related species** section).

A total of 14,701,439 SNPs were identified without missing data. Population structure was evaluated using a principal component analysis (PCA) performed using Ade4 [90] on a set of LD-pruned SNPs without missing data (1,739,037 SNPs) identified stringently with plink1.9 [91] (command indep-pairwise 100 50 0.1).

Outgroup dataset. In order to test the generality of the relationship observed between π_N/π_S and GC3 we took advantage of the newly assembled reference genomes and resequencing data from other closely related Pacific salmonid species with similar demographic histories [92–94]. Sockeye salmon published by [92] were retrieved from NCBI PRJNA530256. Samples with a high number of individuals per ecotype (Sockeye and Kokanee) were chosen from the NCBI table. We retained a total of 5 Kokanee populations and 5 Sockeye populations (from Fraser & Columbia watershed described in **S1 and S3 Tables**). Three Chinook salmon samples were provided by B. Koop (also available at NCBI PRJNA694998). Additionally, 11 samples of "even" and 10 samples of "odd" pink salmon (*O. gorbuscha*) were downloaded from PRJNA 556728 and included in the analysis. Here "even" and "odd" refers to Salmon returning to their natal rivers in "even" and "odd" years to spawn, leading to a temporal isolation of these ecotypes [93]. These were indeed clearly separated based on a PCA. Finally, a number of rainbow trout available from NCBI PRJNA386519 were used (n = 19 from 3 random populations showing genomic differentiation based on a PCA).

Each sample was downloaded and mapped onto its species' reference genome downloaded from NCBI and using the exact same procedure as described above relying on fastp, bwa-mem2, picard and GATK 4.2.5.0 to generate a final vcf filter based on usual GATK quality criteria and variance in sequencing depth. For each species, we then quantified the load using the π_N/π_s ratio with the procedure described below for Coho salmon. For the Sockeye/Kokanee ecotypes, the Sockeye is a fully migratory ecotype, whereas the Kokanee is a resident (non-migratory) ecotype that typically comprises more isolated populations. The two alternative ecotypes are sometimes found in similar locations, with three rivers from our sampling design including both ecotypes (S3 Table). For all other species we tested the relationship between π_N/π_S and GC3 (see below).

Ancestral and derived alleles identification

To accurately recover the ancestral allelic states, we used three outgroup species; including the chinook salmon and rainbow trout sample (see above, n = 5 for rainbow trout) plus data from Atlantic salmon (n = 5, SRP059652). Each individual was aligned against the Coho salmon V2 genome (GCF_002021745.2) using GATK with the same procedure as above and calling every SNP using the–all-site mode to obtain invariant positions. We then determined the ancestral

state of each SNP if 1) the SNP was homozygous in at least 90% of the individuals from our three outgroups, and 2) matched one of the two alleles identified in Coho salmon. Otherwise, the site was inferred as missing and was not used in subsequent analyses of the load. In addition, we reconstructed a consensus ancestral fasta sequence using the doFasta option from angsd [95]. This was used for demographic reconstruction detailed in **S1 Note.**

Demographic reconstruction

We first tested our prediction that genetic diversity (observed heterozygosity H_o) decreases towards the North following our «out of Cascadia» model previously inferred [42, 43]. Conversely, we verified that the β_{ST} coefficient, a measure of both genetic differentiation and ancestrality [46] increases northwards the North, as expected due to isolation by distance. β_{ST} and observed heterozygosity (H_o) were measured using the hierfstat R package [96] Details about β_{ST} computation are provided in Weir & Goudet [46] and H_o was computed following Nei (1987)[97] as $1 - \Sigma_k\Sigma_i Pkii/np$ with $Pkii$ the proportion of homozygotes i in sample k and np the number of samples. Oceanic coastal distances were computed using the marmap package [98] and waterway distance was computed using ArcGIS. Then we summed the 2 distances to obtain the distance to the most likely refugia that we identified in our previous studies [42, 43]. A shapefile of the rivers used here is available at https://github.com/QuentinRougemont/selection_efficacy/tree/main/00.raw_data.

Under postglacial expansion from a single refugium, the general hypothesis would be that all sampled populations should follow a common temporal trajectory of a population decline (bottleneck due to founder events by few individuals) followed by a (strong) increase in N_e corresponding to the expansion phase. To test this hypothesis, we inferred temporal changes in N_e using SMC++ [50]. SMC++ works similarly to the PSMC model but takes into account the Site Frequency Spectrum (SFS) and is better suited to large sample sizes. Estimates of changes in population size were performed for all populations. To validate the fact that expansions are indeed postglacial, splitting time was estimated between all pairs of samples from different geographic areas based on the joint SFS (n = 75 pairwise comparisons). A generation time of 3.5 years, well documented for Coho, and a mutation rate of $8e^{-9}$ mutation/bp/generation were applied (corresponding to the median substitution rate inferred in Atlantic salmon, J. Wang, Personal communication). We also compared the results to the mean substitution rate of $1.25e^{-8}$ mutation/bp/generation also inferred by Wang.

In addition, pairwise linkage disequilibrium provides valuable information regarding population size and inbreeding. We computed the squared correlation coefficient between genotypes in each sample and all populations separately using popLDdecay [99]. We used a MAF of 5% in each population, keeping between 3.7 and 6.4 million SNPs with populations having undergone stronger bottleneck/founding events displaying the lowest amount of variation. We estimated LD decay by plotting LD (R^2) against physical distance measured in base pairs in ggplot2 [100] package in R.

We observed slight discrepancies between our SMC++ estimates of divergence time and our previous work based on the site frequency spectrum [42]. To investigate this, we performed a new set of inference based on the unfolded joint site frequency spectrum (jSFS) using $\partial a \partial i$ [101] and a new set of refined models as detailed in **supp. S1 Note and S8 and S9 Tables**.

To reconstruct the population expansion routes we computed Weir and Cockerham [102] F_{ST} values among populations using Vcftools [103] and constructed a phylogenetic population tree using the R package ape [104]. We projected the tree on the map using the functions contMap and phylo.to.map from the phytools R package [105]. We then computed the tree branch

lengths to the root using the function distroot from adephylo [106]. We also explored broad relationships among populations with treemix [49]. We fitted a model with an increasing number of migration edges. We chose a model with K = 3 migration edges as all edges displayed significant p-value and captured a high proportion of explained variance. Fitting more edges decreased the p-value without really improving the fit to our data. Similarly, we computed the tree branch length to the root using the function adephylo and compared our results to those from F_{ST}-based values. The resulting tree branch length values were used as a proxy for the expansion routes, and we tested their correlation using linear models in R, with all our metrics of deleterious load (π_N/π_S, total number of putative homozygous derived deleterious alleles (recessive load) and total number of deleterious alleles (both in homozygous and heterozygous states, additive load) for derived missense and LoF mutations) and metrics of selection efficacy (ω_{NA}, ω_A, α detailed below). Similar inference was performed, but using the reconstructed distances to the southernmost site included in our previous studies [42, 43]. This distance was computed by summing the oceanographic distance and river distances described above.

Population-scaled recombination rate

Statistical phasing of the Coho whole genome sequences was performed using the Shapeit software [107], considering all individuals at once. We then estimated effective recombination rates ($\rho = 4.N_e.r$ where r represents the recombination rate per generation and N_e is the effective population size) along the genome using LDHat [108]. Phased genotypes were converted into LDHat format using vcftools after excluding SNPs with MAF < 10% since rare variants are not informative for such inferences. Following the guidelines of the LDHat manual, the genome was split into fragments of 2,000 SNPs with overlapping windows of 500 SNPs. We measured recombination rates independently for each population. Differences in the distribution of population-scaled recombination was visualized using violin plot (**S13 Fig**) and statistically tested using Tuckey HSD tests in R (**S5 Table**).

Genetic load estimation

π_N/π_S estimates.   The approach developed in [59] was used to reconstruct fasta sequences for each individual. For each species (Coho and the other salmonids), coding sequences (CDS) from each reconstructed sequence were extracted using the gff files available with the reference genome to estimate the nucleotide diversity (π). We also concatenated the CDS sequences into different classes according to their length and computed π_N and π_S over 4-Mb concatenated gene space windows. Such large windows reduce the stochasticity due to the low π_S values in Coho salmon.

Identifying potential deleterious non-synonymous alleles

We tested the difference in count of non-synonymous mutations in each local population of Coho salmon across non-synonymous missense mutations (putatively deleterious) and Loss of Function (LoF) mutations (likely to be strongly deleterious) identified with SNPeff. We analyzed data in two ways: first, we counted the total number of putative homozygous derived deleterious alleles (recessive load) per individual as well as the total number of deleterious alleles (both in homozygous and heterozygous states, additive load) using: Ntotal = 2 X N_{homo} + N_{hetero} [28]. These individual values were then averaged per population. We tested for differences in the distribution of these counts among populations using an ANOVA followed by a TukeyHSD test. The p-values were corrected using a Bonferroni correction. We also computed mean derived allele frequencies (DAF) in all sampling locations and across mutation categories

(synonymous, non-synonymous missense and LoF). We also applied the commonly used Provean [109] software based on a random set of non-synonymous mutations (but see **S3 Note** for a brief discussion regarding the limitations).These results were then compared with results from non-synonymous mutations (**S15 Fig**).

Correlation between π_N/π_S and recombination

We computed the GC content at third-codon positions of protein coding genes (GC3) which has been shown to be an accurate proxy of local recombination rate in other species and these positions are generally silent [85, 86]. To compute π_N/π_S values we sorted genes by ascending GC3 values, which enabled us to obtain a ratio based on genes with similar GC3 values. Moreover, we also used the site frequency-based approach proposed by Rousselle et al. [60] to estimate the π_N/π_S ratios. This approach enabled us to compute SFS separately for GC conservative sites (A<->T and C<->G mutations), that is, not affected by GC-biased Gene Conversion (gBGC).

Finally, we measured the correlation between GC3 and π_N/π_S using linear models. We replicated these analyses considering only genes (n = 3,500) and SNPs in regions of residual tetraploidy (8% of the genome).

DFE estimation and rate of adaptation in Coho salmon

We estimated the rate of non-adaptive and adaptive synonymous substitutions (ω_{NA} and ω_A, respectively; with $\omega_A = d_N/d_S - \omega_{NA}$) and the proportion of amino-acid substitution potentially resulting from positive selection ($\alpha = \omega_A/(d_N/d_S)$, with d_N being the rate of non-synonymous substitutions, d_S being the rate of synonymous substitutions). To do so, we used the method implemented in Grapes v1.0 which builds upon the approach of [110]. Grapes models the effect of favorable mutations on the non-synonymous site frequency spectrum (SFS) while accounting for various confounding factors distorting the SFS (demographic change, linked selection, genotyping errors, SNP misorientation).

We used the following parameters in Grapes v1.0: we assumed a negative Gamma distribution to the synonymous and non-synoymous SFS (parameters GammaExpo in Grapes and parameter "unfolded" site frequency spectrum). To obtain suitable data, we converted the quality filtered whole genome vcf file into a fasta file for each population containing sequence information for each individual in the population (using vcf2fasta available at https://github.com/QuentinRougemont/selection_efficacy/tree/main/08.piNpiS/). This file was then converted into a site-frequency spectrum using bppml [111]. We required at least 10 sites without gap to keep a given site (-gapN_site), with a maximum proportion of gap of 0.5 (-gapN_seq), a minimum number of complete codon of 6 (-min_nb_codon), we did not allow frameshift (remove_frameshift parameter), we also required a sample size of 8 (-sample_size), the number of initial/terminal position in which Stop codons or FrameShift codons are tolerated was set to 20 (-tolerance_zone), we did not allow Stop or FrameShift codons between the two tolerance zones (-allow_internal_bc parameter). The kappa value (i.e Ts/Tv ratio) was set to 1.6 and we used an unfolded SFS using the three species as an outgroup. Fitted parameters of the DFE were used to compute the expected d_N/d_S under near neutrality, which was compared to the observed d_N/d_S to estimate α, ω_{NA}, ωa.

Differences in load for region of residual tetraploidy in Coho salmon

π_N/π_S comparison. In the Coho reference genome, Chromosomes 1 to 30 are considered to represent generally diploid chromosomes, whereas chromosomes 31 to 38 represent those with a clear signal of residual tetraploid *[41]*. We took advantage of this specificity regarding

chromosome evolution to contrast the load for the 3700 genes in regions of residual tetraploidy (averaged across all genes for each population). For diploid regions, we generated 200 datasets of 4,000 genes randomly sampled and then estimated the load for each of these datasets.

TE annotations

We used the TEs annotation file from repeatmasker [112] (made available on NCBI for the reference genome [41]) and tested for difference in the length of TEs between diploid and tetraploid regions, after correcting for the difference in chromosome length.

Supporting information

S1 Table. Sampling strategy, including various outgroup species.
(XLS)

S2 Table. Summary Statistics across coho populations, including geographic coordinates, tree branch length, genetic diversity and load statistics. Fig 1 to Fig 4 can be reconstructed from these.
(XLS)

S3 Table. Outgroup summary statistics by species, with a focus on the load.
(XLS)

S4 Table. Results of linear models. These provide tests of the relationship between branch length of the population phylogenies based on (a) pairwise Fst value and b) treemix tree inferred with 3 migrations event. c) treemix results obtained after removing the "salmon" river with aberrant branch length.
(XLS)

S5 Table. Results of Mann-Whitney test for difference in load among population based on missense mutation and Loss of Function mutation. Mutation effect identified with SNPeff.
(XLS)

S6 Table. Results of Tukey-HSD test for difference in recombination rate among populations based on Ldhat estimates. "Pair" is the compared population pair with the initial described in Table S01. "Diff" is the difference in recombination between the pair Lower and Upper CI are the 95% confidence level
(XLS)

S7 Table. Difference in load among diploid region, compared to region of residual tetraploidy with load computed in 500kb windows for each kind of regions.
(XLS)

S8 Table. AIC of each model for each pairwise comparison. AM = Ancient Migration, IM = Isolation With Migration, SI = Strict Isolation, SC = Secondary Contact, G = prefix indicating Growth in the descending population, 2N = prefix indicating linked selection, 2m = prefix indicating reduced effective migration along the genome, the A prefix after each model (e.g. AM<u>A</u>) indicated a Growth in the ancestral population.
(XLS)

S9 Table. Parameter estimates for each of the major regional group where $\partial a \partial i$ was fitted. Na = effective size of the ancestral population, Ne pop1 = effective size of the first population, Nepop2 = effective size of the second population, m12 = migration rate from 2 into 1, m21 being the reverse, me12 = effective migration rate in barriers regions, me21 being the same in

the reverse, Tsplit = Split time, Tam = time of migration stop, P = proportion of the genome being neutrally exchanged, Q = proportion the genome undergoing linked selection, O = proportion of the genome correctly oriented, hrf = Hill-Roberston factor, indicating the extent of reduction in Ne in region affected by linked selection, b1, b2 = extend of population growth in current population1 and 2 respectively.
(XLS)

S1 Note. Reconstruction of demographic history from RADseq data.
(ODT)

S2 Note. Relationship between GC3 and recombination.
(ODT)

S3 Note. Comparison of Provean and non-synonymous results.
(ODT)

S1 Fig. PCA and admixture plots among population. A. Result of a principal component analysis obtained from a set of high quality biallelic SNPs without missing data showing both a clusterization along latitude and longitude as well as discrete clusters corresponding broadly to each river. Each label represents a given individual from a given river (labelled following table S01) and is coloured according to its region of sampling. B. LEA results for admixture inference for K = 14. Each bar represents an individual and is coloured according to its membership probability. Each name corresponds to a river. The TsooYes appear as a mixture of different individuals. Results must be interpreted with caution given the small sample sizes.
(TIF)

S2 Fig. Summary statistics revealed the demography of Coho salmon. A. Positive correlation between the β_{ST} and distance to the southernmost site showing that differentiation increased linearly from the south to the north. In all panels each point represents a sampling site and is coloured according to the region in which it was sampled. The most negative values display likely ancestral samples. The Thompson sample displays high inbreeding and is bottlenecked. Displayed is the adjusted R^2 of a linear model along with its *p-value*. The grey area represents the 95% confidence interval levels around the regression lines obtained with the predict function in R. B. Negative correlation between genetic diversity (observed heterozygosity) and distance to the south.The Thompson sample displays high inbreeding and is bottlenecked. Displayed is the adjusted R^2 of a linear model along with its *p-value*. The grey area represents the 95% confidence interval levels around the regression lines obtained with the predict function in R. C. Rates of LD decay as a function of distance along the genome. The higher LD indicates a history of inbreeding or bottleneck. D. SMC++ inference of population size change with whole genome sequences for each local population of Coho salmon. Recent times should be interpreted carefully.
(TIF)

S3 Fig. Inference of population split and mixture from Treemix. A) Tree with three migration arrows. Each name describes a river sample site. Each river is color coded following the color scheme provided elsewhere (e.g. Fig 1). 3 significant migration arrows are displayed. Each migration arrow is colored according to the weight it received (from yellow to red) in Treemix. The weights are related to the fraction of alleles in the descendant population that originated in each donor population. Each node was highly supported based on 500 bootstrap. B) proportion of variance in the covariance of allele frequency explained as a function of the number of migration edges. C) Same tree colored according to the values of π_N/π_S
(TIF)

S4 Fig. SMC++ split time. Estimates of population split time from SMC++ under a model without gene flow among populations. Shown are estimates obtained when comparing split time between pairs of samples from different major regional groups. Two different mutation rates were used the: mean and median values based on *Salmo salar* orthologues mapped on the pike *Esox lucius* genome (Wang J. personal communication).
(TIF)

S5 Fig. Correlation between π_N/π_S and π_S and π_N/π_S and N_e from smc++. A) Distribution of π_N/π_S as a function of π_S in each coho salmon populations from the study. B) Distribution of π_N/π_S as a function of N_e from SMC++ for each coho salmon populations from the study. Results of linear models are displayed. In all panels each point represents a sampling site and is coloured according to the region in which it was sampled. Displayed is the adjusted R^2 of a linear model along with its *p-value*. The grey area represents the 95% confidence interval levels around the regression lines obtained with the predict function in R.+
(TIF)

S6 Fig. Correlation between distance to the ocean of each sample location (i.e. corresponding to the spawning migration) and the inferred rate of **A)** non-adaptive substitution (ω_{NA}) and **B)** adaptive substitution (ω_A). In all panels each point represents a sampling site and is coloured according to the region in which it was sampled. Displayed is the adjusted R^2 of a linear model along with its p-value. The grey area represents the 95% confidence interval levels around the regression lines obtained with the predict function in R.
(TIF)

S7 Fig. Results of linear models testing the effect of tree branch length to the root extracted from a F_{ST}-based population phylogeny on different metrics of selection efficacy. A: relationship between ω_{NA} and tree branch length; **B:** relationship between ω_A and tree branch length; **C:** relationship between α and tree branch length. See text for a definition of each metrics. Sample sites are coloured by region. The blue line represents the value of the regression line. In all panels each point represents a sampling site and is coloured according to the region in which it was sampled. Displayed is the adjusted R^2 along with its p-value.
(TIF)

S8 Fig. Results of linear models testing the effect of tree branch length to the root extracted from a treemix population phylogeny on the load (π_N/π_S, panel A) and different metrics of selection efficacy B: relationship between ω_{NA} and tree branch length; **C:** relationship between ω_A and tree branch length; **D:** relationship between α and tree branch length. See text for a definition of each metrics). Sample sites are coloured by region. The blue line represents the value of the regression line. In all panels each point represents a sampling site and is coloured according to the region in which it was sampled. Displayed is the adjusted R^2 along with its p-value.
(TIF)

S9 Fig. Correlation between the proportion of amino-acid substitution that results from positive selection (α) and the synonymous diversity π_S used as a proxy of effective population size. Each point represents a sampling site and is coloured according to the region in which it was sampled. Displayed is the adjusted R^2 along with its p-value. The grey area represents the 95% confidence interval levels around the regression lines obtained with the predict function in R.
(TIF)

S10 Fig. Relationship between GC3 and pN/pS for all populations and all outgroups. A) Correlation for each population of coho salmon. Each point represents a sampling site and is coloured according the region in which it was sampled; **B**) correlation within populations of rainbow trout. Each point represent a population as infered using a PCA and corresponds to different rivers of sampling. **C**) correlation for each population of Sockeye and Kokanee ecotype. Each point corresponds to differents rivers. All correlations are significant. The x-axis displays the median GC3 and y-axis the π_N/π_S ratio. Abbreviation for each site is available in Table S01. Displayed is the adjusted R^2 of a linear model along with its *p-value*. The grey area represents the 95% confidence interval levels around the regression lines obtained with the predict function in R.
(TIFF)

S11 Fig. Relationship between recombination (GC3) and demographic factors (distance to the southernmost site). **A)** relationship between the slope of the linear model between GC3 ~ and π_N/π_S and the distance to the southernmost site. **B)** Correlation between the lowest recombining GC3 classes (expected to display the highest load) and the distance to the southernmost sites. In all panels each point represents a sampling site and is coloured according to the region in which it was sampled. Displayed is the adjusted R^2 of a linear model along with its *p-value*. The grey area represents the 95% confidence interval levels around the regression lines obtained with the predict function in R.
(TIFF)

S12 Fig. Region of residual tetraploidy vs diploid region of the genome display different recombination landscapes. Combined Violin plot and boxplot showing the distribution of population scale recombination ($\rho = 4*N_e*r$) inferred from LDhat in Diploid chromosomes (orange) *vs* the 8 Regions of residual tetraploidy (gray).
(TIF)

S13 Fig. Distribution of recombination rate among all populations. Each point represents the observed value of population scale recombination rate ($\rho = 4N_e*\mu$) computed in 1 mb windows over the whole genome in each population. The harmonic mean is plotted by a red dot along with its value. For each population a violin plot embedded within a boxplot is shown.
(TIF)

S14 Fig. TE length differs between diploid chromosome versus chromosome displaying residual tetraploidy. Violin plot displaying the difference in TEs relative length (i.e. length corrected by the total length of each chromosome) for each major TE category and each type of chromosome. Red point = mean +/- 1*sd.
(TIFF)

S15 Fig. Provean analysis of potentially deleterious mutation and the resulting load. *Boxplot showing the number of deleterious alleles per river (sorted from the south to to north). left panel = additive load, right panel = recessive load. top = missense deleterious mutations according to Provean predictions, bottom = missense tolerated mutations according to Provean predictions*. No strong differences are observed in the additive load among populations. Significant differences were observed for the recessive load in populations at the expansion front which is qualitatively similar to our inferences from missense and LoF mutations. Each color represents a major regional group. Results were obtained for a random subset of mutations only given the strong computational burden of Provean.
(TIF)

Acknowledgments

Author Contributions

Conceptualization: Quentin Rougemont, Louis Bernatchez.

Data curation: Quentin Rougemont.

Formal analysis: Quentin Rougemont, Thibault Leroy.

Funding acquisition: Louis Bernatchez.

Investigation: Quentin Rougemont.

Methodology: Quentin Rougemont.

Project administration: Louis Bernatchez.

Resources: Eric B. Rondeau, Ben Koop.

Software: Quentin Rougemont.

Supervision: Louis Bernatchez.

Visualization: Quentin Rougemont.

Writing – original draft: Quentin Rougemont.

Writing – review & editing: Thibault Leroy, Louis Bernatchez.

References

1. Hewitt GM. Genetic consequences of climatic oscillations in the Quaternary. Philos Trans R Soc Lond, B, Biol Sci. 2004; 359: 183–195; discussion 195. https://doi.org/10.1098/rstb.2003.1388 PMID: 15101575

2. Excoffier L, Foll M, Petit RJ. Genetic Consequences of Range Expansions. Annual Review of Ecology, Evolution, and Systematics. 2009; 40: 481.

3. Slatkin M, Excoffier L. Serial Founder Effects During Range Expansion: A Spatial Analog of Genetic Drift. Genetics. 2012; 191: 171–181. https://doi.org/10.1534/genetics.112.139022 PMID: 22367031

4. Ohta T. Linkage disequilibrium due to random genetic drift in finite subdivided populations. Proc Natl Acad Sci U S A. 1982; 79: 1940–1944. https://doi.org/10.1073/pnas.79.6.1940 PMID: 16593171

5. Hallatschek O, Hersen P, Ramanathan S, Nelson DR. Genetic drift at expanding frontiers promotes gene segregation. Proc Natl Acad Sci U S A. 2007; 104: 19926–19930. https://doi.org/10.1073/pnas.0710150104 PMID: 18056799

6. Klopfstein S, Currat M, Excoffier L. The Fate of Mutations Surfing on the Wave of a Range Expansion. Molecular Biology and Evolution. 2006; 23: 482–490. https://doi.org/10.1093/molbev/msj057 PMID: 16280540

7. Travis JMJ, Münkemüller T, Burton OJ, Best A, Dytham C, Johst K. Deleterious Mutations Can Surf to High Densities on the Wave Front of an Expanding Population. Molecular Biology and Evolution. 2007; 24: 2334–2343. https://doi.org/10.1093/molbev/msm167 PMID: 17703053

8. Peischl S, Dupanloup I, Kirkpatrick M, Excoffier L. On the accumulation of deleterious mutations during range expansions. Mol Ecol. 2013; 22: 5972–5982. https://doi.org/10.1111/mec.12524 PMID: 24102784

9. Peischl S, Excoffier L. Expansion load: recessive mutations and the role of standing genetic variation. Molecular Ecology. 2015; 24: 2084–2094. https://doi.org/10.1111/mec.13154 PMID: 25786336

10. Peischl S, Dupanloup I, Foucal A, Jomphe M, Bruat V, Grenier J-C, et al. Relaxed Selection During a Recent Human Expansion. Genetics. 2018; 208: 763–777. https://doi.org/10.1534/genetics.117.300551 PMID: 29187508

11. Haag CR, Roze D. Genetic Load in Sexual and Asexual Diploids: Segregation, Dominance and Genetic Drift. Genetics. 2007; 176: 1663–1678. https://doi.org/10.1534/genetics.107.073080 PMID: 17483409

12. Ohta T. Slightly Deleterious Mutant Substitutions in Evolution. Nature. 1973; 246: 96–98. https://doi.org/10.1038/246096a0 PMID: 4585855

13. Hedrick PW, Garcia-Dorado A. Understanding Inbreeding Depression, Purging, and Genetic Rescue. Trends in Ecology & Evolution. 2016; 31: 940–952. https://doi.org/10.1016/j.tree.2016.09.005 PMID: 27743611

14. Simons YB, Sella G. The impact of recent population history on the deleterious mutation load in humans and close evolutionary relatives. Curr Opin Genet Dev. 2016; 41: 150–158. https://doi.org/10.1016/j.gde.2016.09.006 PMID: 27744216

15. Lohmueller KE. The Impact of Population Demography and Selection on the Genetic Architecture of Complex Traits. Williams SM, editor. PLoS Genet. 2014; 10: e1004379. https://doi.org/10.1371/journal.pgen.1004379 PMID: 24875776

16. Willi Y, Fracassetti M, Zoller S, Van Buskirk J. Accumulation of Mutational Load at the Edges of a Species Range. Mol Biol Evol. 2018; 35: 781–791. https://doi.org/10.1093/molbev/msy003 PMID: 29346601

17. Willi Y, Fracassetti M, Bachmann O, Van Buskirk J. Demographic Processes Linked to Genetic Diversity and Positive Selection across a Species' Range. Plant Communications. 2020; 1: 100111. https://doi.org/10.1016/j.xplc.2020.100111 PMID: 33367266

18. Perrier A, Sánchez-Castro D, Willi Y. Expressed mutational load increases toward the edge of a species' geographic range. Evolution. 2020; 74: 1711–1723. https://doi.org/10.1111/evo.14042 PMID: 32538471

19. de Pedro M, Riba M, González-Martínez SC, Seoane P, Bautista R, Claros MG, et al. Demography, genetic diversity and expansion load in the colonizing species Leontodon longirostris (Asteraceae) throughout its native range. Molecular Ecology. 2021; 30: 1190–1205. https://doi.org/10.1111/mec.15802 PMID: 33452714

20. González-Martínez SC, Ridout K, Pannell JR. Range Expansion Compromises Adaptive Evolution in an Outcrossing Plant. Current Biology. 2017; 27: 2544–2551.e4. https://doi.org/10.1016/j.cub.2017.07.007 PMID: 28803874

21. Lucek K, Willi Y. Drivers of linkage disequilibrium across a species' geographic range. PLOS Genetics. 2021; 17: e1009477. https://doi.org/10.1371/journal.pgen.1009477 PMID: 33770075

22. Bosshard L, Dupanloup I, Tenaillon O, Bruggmann R, Ackermann M, Peischl S, et al. Accumulation of Deleterious Mutations During Bacterial Range Expansions. Genetics. 2017; 207: 669–684. https://doi.org/10.1534/genetics.117.300144 PMID: 28821588

23. Takou M, Hämälä T, Koch EM, Steige KA, Dittberner H, Yant L, et al. Maintenance of Adaptive Dynamics and No Detectable Load in a Range-Edge Outcrossing Plant Population. Molecular Biology and Evolution. 2021; 38: 1820–1836. https://doi.org/10.1093/molbev/msaa322 PMID: 33480994

24. Rousselle M, Simion P, Tilak M-K, Figuet E, Nabholz B, Galtier N. Is adaptation limited by mutation? A timescale-dependent effect of genetic diversity on the adaptive substitution rate in animals. PLoS Genet. 2020; 16: e1008668. https://doi.org/10.1371/journal.pgen.1008668 PMID: 32251427

25. Lanfear R, Kokko H, Eyre-Walker A. Population size and the rate of evolution. Trends Ecol Evol. 2014; 29: 33–41. https://doi.org/10.1016/j.tree.2013.09.009 PMID: 24148292

26. McDonald JH, Kreitman M. Adaptive protein evolution at the Adh locus in Drosophila. Nature. 1991; 351: 652–654. https://doi.org/10.1038/351652a0 PMID: 1904993

27. Laenen B, Tedder A, Nowak MD, Toräng P, Wunder J, Wötzel S, et al. Demography and mating system shape the genome-wide impact of purifying selection in Arabis alpina. PNAS. 2018; 115: 816–821. https://doi.org/10.1073/pnas.1707492115 PMID: 29301967

28. Henn BM, Botigué LR, Peischl S, Dupanloup I, Lipatov M, Maples BK, et al. Distance from sub-Saharan Africa predicts mutational load in diverse human genomes. PNAS. 2016; 113: E440–E449. https://doi.org/10.1073/pnas.1510805112 PMID: 26712023

29. Do R, Balick D, Li H, Adzhubei I, Sunyaev S, Reich D. No evidence that selection has been less effective at removing deleterious mutations in Europeans than in Africans. Nat Genet. 2015; 47: 126–131. https://doi.org/10.1038/ng.3186 PMID: 25581429

30. Felsenstein J. The evolutionary advantage of recombination. Genetics. 1974; 78: 737–756. https://doi.org/10.1093/genetics/78.2.737 PMID: 4448362

31. Nordborg M, Charlesworth B, Charlesworth D. The effect of recombination on background selection. Genet Res. 1996; 67: 159–174. https://doi.org/10.1017/s0016672300033619 PMID: 8801188

32. Muller HJ. The relation of recombination to mutational advance. Mutation Research/Fundamental and Molecular Mechanisms of Mutagenesis. 1964; 1: 2–9. https://doi.org/10.1016/0027-5107(64)90047-8 PMID: 14195748

33. Hill WG, Robertson A. The effect of linkage on limits to artificial selection. Genetics Research. 1966; 8: 269–294. https://doi.org/10.1017/S0016672300010156 PMID: 5980116

34. Hill RR. Selection in autotetraploids. Theor Appl Genet. 1970; 41: 181–186. https://doi.org/10.1007/BF00277621 PMID: 24430193

35. Baduel P, Bray S, Vallejo-Marin M, Kolář F, Yant L. The "Polyploid Hop": Shifting Challenges and Opportunities Over the Evolutionary Lifespan of Genome Duplications. Frontiers in Ecology and Evolution. 2018; 6. Available: https://www.frontiersin.org/articles/10.3389/fevo.2018.00117.

36. Monnahan P, Brandvain Y. The effect of autopolyploidy on population genetic signals of hard sweeps. Biology Letters. 2020; 16: 20190796. https://doi.org/10.1098/rsbl.2019.0796 PMID: 32097595

37. Baduel P, Quadrana L, Hunter B, Bomblies K, Colot V. Relaxed purifying selection in autopolyploids drives transposable element over-accumulation which provides variants for local adaptation. Nat Commun. 2019; 10: 5818. https://doi.org/10.1038/s41467-019-13730-0 PMID: 31862875

38. Monnahan P, Kolář F, Baduel P, Sailer C, Koch J, Horvath R, et al. Pervasive population genomic consequences of genome duplication in Arabidopsis arenosa. Nat Ecol Evol. 2019; 3: 457–468. https://doi.org/10.1038/s41559-019-0807-4 PMID: 30804518

39. Sergeant CJ, Sexton EK, Moore JW, Westwood AR, Nagorski SA, Ebersole JL, et al. Risks of mining to salmonid-bearing watersheds. Science Advances. 2022; 8: eabn0929. https://doi.org/10.1126/sciadv.abn0929 PMID: 35776798

40. Gustafson RG, Waples RS, Myers JM, Weitkamp LA, Bryant GJ, Johnson OW, et al. Pacific Salmon Extinctions: Quantifying Lost and Remaining Diversity. Conservation Biology. 2007; 21: 1009–1020. https://doi.org/10.1111/j.1523-1739.2007.00693.x PMID: 17650251

41. Rondeau EB, Christensen KA, Minkley DR, Leong JS, Chan MTT, Despins CA, et al. Population-size history inferences from the coho salmon (Oncorhynchus kisutch) genome. G3 Genes|Genomes|Genetics. 2023; 13: jkad033. https://doi.org/10.1093/g3journal/jkad033 PMID: 36759939

42. Rougemont Q, Moore J-S, Leroy T, Normandeau E, Rondeau EB, Withler RE, et al. Demographic history shaped geographical patterns of deleterious mutation load in a broadly distributed Pacific Salmon. PLOS Genetics. 2020; 16: e1008348. https://doi.org/10.1371/journal.pgen.1008348 PMID: 32845885

43. Rougemont Q, Xuereb A, Dallaire X, Moore J-S, Normandeau E, Perreault-Payette A, et al. Long-distance migration is a major factor driving local adaptation at continental scale in Coho salmon. Molecular Ecology. 2023; 32: 542–559. https://doi.org/10.1111/mec.16339 PMID: 35000273

44. Macqueen DJ, Johnston IA. A well-constrained estimate for the timing of the salmonid whole genome duplication reveals major decoupling from species diversification. Proc Biol Sci. 2014;281. https://doi.org/10.1098/rspb.2013.2881 PMID: 24452024

45. Novembre J, Stephens M. Interpreting principal component analyses of spatial population genetic variation. Nat Genet. 2008; 40: 646–649. https://doi.org/10.1038/ng.139 PMID: 18425127

46. Weir BS, Goudet J. A Unified Characterization of Population Structure and Relatedness. Genetics. 2017; 206: 2085–2103. https://doi.org/10.1534/genetics.116.198424 PMID: 28550018

47. natural earth data. https://www.naturalearthdata.com/http/www.naturalearthdata.com/download/110m/physical/110m_physical.zip.

48. Hill WG, Robertson A. Linkage disequilibrium in finite populations. Theor Appl Genet. 1968; 38: 226–231. https://doi.org/10.1007/BF01245622 PMID: 24442307

49. Pickrell JK, Pritchard JK. Inference of Population Splits and Mixtures from Genome-Wide Allele Frequency Data. PLOS Genetics. 2012; 8: e1002967. https://doi.org/10.1371/journal.pgen.1002967 PMID: 23166502

50. Terhorst J, Kamm JA, Song YS. Robust and scalable inference of population history from hundreds of unphased whole genomes. Nature Genetics. 2017; 49: 303–309. https://doi.org/10.1038/ng.3748 PMID: 28024154

51. world Hire data. worldHires data public domain https://www.evl.uic.edu/pape/data/WDB/namer.tar.gz).

52. Gravel S. When Is Selection Effective? Genetics. 2016; 203: 451–462. https://doi.org/10.1534/genetics.115.184630 PMID: 27010021

53. Brandvain Y, Wright SI. The Limits of Natural Selection in a Nonequilibrium World. Trends in Genetics. 2016; 32: 201–210. https://doi.org/10.1016/j.tig.2016.01.004 PMID: 26874998

54. Bertorelle G, Raffini F, Bosse M, Bortoluzzi C, Iannucci A, Trucchi E, et al. Genetic load: genomic estimates and applications in non-model animals. Nat Rev Genet. 2022; 23: 492–503. https://doi.org/10.1038/s41576-022-00448-x PMID: 35136196

55. Kyriazis C, Wayne RK, Lohmueller KE. High genetic diversity can contribute to extinction in small populations | bioRxiv. 10 Mar 2020 [cited 10 Mar 2020]. Available: https://www.biorxiv.org/content/10.1101/678524v1.

56. Galtier N. Adaptive Protein Evolution in Animals and the Effective Population Size Hypothesis. PLOS Genetics. 2016; 12: e1005774. https://doi.org/10.1371/journal.pgen.1005774 PMID: 26752180

57. Ryman N, Laikre L. Effects of Supportive Breeding on the Genetically Effective Population Size. Conservation Biology. 1991; 5: 325–329. https://doi.org/10.1111/j.1523-1739.1991.tb00144.x

58. Berdan EL, Blanckaert A, Butlin RK, Bank C. Deleterious mutation accumulation and the long-term fate of chromosomal inversions. PLOS Genetics. 2021; 17: e1009411. https://doi.org/10.1371/journal.pgen.1009411 PMID: 33661924

59. Leroy T, Rousselle M, Tilak M-K, Caizergues AE, Scornavacca C, Recuerda M, et al. Island songbirds as windows into evolution in small populations. Current Biology. 2021 [cited 3 Mar 2021]. https://doi.org/10.1016/j.cub.2020.12.040 PMID: 33476557

60. Rousselle M, Laverré A, Figuet E, Nabholz B, Galtier N. Influence of Recombination and GC-biased Gene Conversion on the Adaptive and Nonadaptive Substitution Rate in Mammals versus Birds. Mol Biol Evol. 2019; 36: 458–471. https://doi.org/10.1093/molbev/msy243 PMID: 30590692

61. MacPherson B, Scott R, Gras R. Sex and recombination purge the genome of deleterious alleles: An Individual Based Modeling Approach. Ecological Complexity. 2021; 45: 100910. https://doi.org/10.1016/j.ecocom.2021.100910

62. Kent TV, Uzunović J, Wright SI. Coevolution between transposable elements and recombination. Philosophical Transactions of the Royal Society B: Biological Sciences. 2017; 372: 20160458. https://doi.org/10.1098/rstb.2016.0458 PMID: 29109221

63. Xuereb A, Rougemont Q, Dallaire X, Moore J-S, Normandeau E, Bougas B, et al. Re-evaluating Coho salmon (Oncorhynchus kisutch) conservation units in Canada using genomic data. Evolutionary Applications. 2022; 15: 1925–1944. https://doi.org/10.1111/eva.13489 PMID: 36426130

64. Government of Canada PS and PC. Stock assessment of Thompson River/upper Fraser River coho salmon / J.R. Irvine . . . [et al.].: Fs70-1/1999-28E-PDF—Government of Canada Publications—Canada.ca. 1 Jul 2002 [cited 11 Aug 2022]. Available: https://publications.gc.ca/site/eng/9.804890/publication.html.

65. Waples RS, Hindar K, Karlsson S, Hard JJ. Evaluating the Ryman–Laikre effect for marine stock enhancement and aquaculture. Curr Zool. 2016; 62: 617–627. https://doi.org/10.1093/cz/zow060 PMID: 29491949

66. Gilbert-Horvath EA, Pipal KA, Spence BC, Williams TH, Garza JC. Hierarchical Phylogeographic Structure of Coho Salmon in California. Transactions of the American Fisheries Society. 2016; 145: 1122–1138. https://doi.org/10.1080/00028487.2016.1201003

67. Kratochvíl L, Rovatsos M. Ratios can be misleading for detecting selection. Curr Biol. 2022; 32: R28–R30. https://doi.org/10.1016/j.cub.2021.11.066 PMID: 35015989

68. Leroy T, Nabholz B. Response to Kratochvíl and Rovatsos. Curr Biol. 2022; 32: R30–R31. https://doi.org/10.1016/j.cub.2021.11.067 PMID: 35015990

69. Simons YB, Turchin MC, Pritchard JK, Sella G. The deleterious mutation load is insensitive to recent population history. Nature Genetics. 2014; 46: 220–224. https://doi.org/10.1038/ng.2896 PMID: 24509481

70. Ramu P, Esuma W, Kawuki R, Rabbi IY, Egesi C, Bredeson JV, et al. Cassava haplotype map highlights fixation of deleterious mutations during clonal propagation. Nat Genet. 2017; 49: 959–963. https://doi.org/10.1038/ng.3845 PMID: 28416819

71. Harwood MP, Alves I, Edgington H, Agbessi M, Bruat V, Soave D, et al. Recombination affects allele-specific expression of deleterious variants in human populations. Sci Adv. 8: eabl3819. https://doi.org/10.1126/sciadv.abl3819 PMID: 35559670

72. Hussin JG, Hodgkinson A, Idaghdour Y, Grenier J-C, Goulet J-P, Gbeha E, et al. Recombination affects accumulation of damaging and disease-associated mutations in human populations. Nat Genet. 2015; 47: 400–404. https://doi.org/10.1038/ng.3216 PMID: 25685891

73. Alves I, Houle AA, Hussin JG, Awadalla P. The impact of recombination on human mutation load and disease. Philos Trans R Soc Lond B Biol Sci. 2017; 372: 20160465. https://doi.org/10.1098/rstb.2016.0465 PMID: 29109227

74. Gillard GB, Grønvold L, Røsæg LL, Holen MM, Monsen Ø, Koop BF, et al. Comparative regulomics supports pervasive selection on gene dosage following whole genome duplication. Genome Biology. 2021; 22: 103. https://doi.org/10.1186/s13059-021-02323-0 PMID: 33849620

75. Conover JL, Wendel JF. Deleterious Mutations Accumulate Faster in Allopolyploid Than Diploid Cotton (Gossypium) and Unequally between Subgenomes. Molecular Biology and Evolution. 2022; 39: msac024. https://doi.org/10.1093/molbev/msac024 PMID: 35099532

76. Haldane J. The Causes of Evolution. 1932 [cited 9 Jun 2023]. Available: https://jbshaldane.org/books/1932-Causes-of-Evolution/index.html.

77. Khan A, Patel K, Shukla H, Viswanathan A, van der Valk T, Borthakur U, et al. Genomic evidence for inbreeding depression and purging of deleterious genetic variation in Indian tigers. Proceedings of the National Academy of Sciences. 2021; 118: e2023018118. https://doi.org/10.1073/pnas.2023018118 PMID: 34848534

78. Robinson JA, Räikkönen J, Vucetich LM, Vucetich JA, Peterson RO, Lohmueller KE, et al. Genomic signatures of extensive inbreeding in Isle Royale wolves, a population on the threshold of extinction. Sci Adv. 2019; 5: eaau0757. https://doi.org/10.1126/sciadv.aau0757 PMID: 31149628

79. Grossen C, Guillaume F, Keller LF, Croll D. Purging of highly deleterious mutations through severe bottlenecks in Alpine ibex. Nat Commun. 2020; 11: 1001. https://doi.org/10.1038/s41467-020-14803-1 PMID: 32081890

80. Kleinman-Ruiz D, Lucena-Perez M, Villanueva B, Fernández J, Saveljev AP, Ratkiewicz M, et al. Purging of deleterious burden in the endangered Iberian lynx. Proceedings of the National Academy of Sciences. 2022; 119: e2110614119. https://doi.org/10.1073/pnas.2110614119 PMID: 35238662

81. Parmesan C, Yohe G. A globally coherent fingerprint of climate change impacts across natural systems. Nature. 2003; 421: 37–42. https://doi.org/10.1038/nature01286 PMID: 12511946

82. Irvine JR, Fukuwaka M. Pacific salmon abundance trends and climate change. ICES J Mar Sci. 2011; 68: 1122–1130. https://doi.org/10.1093/icesjms/fsq199

83. Teixeira JC, Huber CD. The inflated significance of neutral genetic diversity in conservation genetics. PNAS. 2021; 118. https://doi.org/10.1073/pnas.2015096118 PMID: 33608481

84. García-Dorado A, Caballero A. Neutral genetic diversity as a useful tool for conservation biology. Conserv Genet. 2021; 22: 541–545. https://doi.org/10.1007/s10592-021-01384-9

85. Kardos M, Armstrong EE, Fitzpatrick SW, Hauser S, Hedrick PW, Miller JM, et al. The crucial role of genome-wide genetic variation in conservation. Proceedings of the National Academy of Sciences. 2021; 118: e2104642118. https://doi.org/10.1073/pnas.2104642118 PMID: 34772759

86. Ripple WJ, Wolf C, Newsome TM, Gregg JW, Lenton TM, Palomo I, et al. World Scientists' Warning of a Climate Emergency 2021. BioScience. 2021; 71: 894–898. https://doi.org/10.1093/biosci/biab079

87. Chen S, Zhou Y, Chen Y, Gu J. fastp: an ultra-fast all-in-one FASTQ preprocessor. Bioinformatics. 2018; 34: i884–i890. https://doi.org/10.1093/bioinformatics/bty560 PMID: 30423086

88. Li H. Aligning sequence reads, clone sequences and assembly contigs with BWA-MEM. arXiv:13033997 [q-bio]. 2013 [cited 3 Jul 2019]. Available: http://arxiv.org/abs/1303.3997.

89. DePristo MA, Banks E, Poplin R, Garimella KV, Maguire JR, Hartl C, et al. A framework for variation discovery and genotyping using next-generation DNA sequencing data. Nature Genetics. 2011; 43: 491. https://doi.org/10.1038/ng.806 PMID: 21478889

90. Dray S, Dufour A-B. The ade4 Package: Implementing the Duality Diagram for Ecologists. Journal of Statistical Software. 2007; 22: 1–20.

91. Purcell S, Neale B, Todd-Brown K, Thomas L, Ferreira MAR, Bender D, et al. PLINK: A Tool Set for Whole-Genome Association and Population-Based Linkage Analyses. Am J Hum Genet. 2007; 81: 559–575. https://doi.org/10.1086/519795 PMID: 17701901

92. Christensen KA, Rondeau EB, Minkley DR, Sakhrani D, Biagi CA, Flores A-M, et al. The sockeye salmon genome, transcriptome, and analyses identifying population defining regions of the genome. PLOS ONE. 2020; 15: e0240935. https://doi.org/10.1371/journal.pone.0240935 PMID: 33119641

93. Christensen KA, Rondeau EB, Sakhrani D, Biagi CA, Johnson H, Joshi J, et al. The pink salmon genome: Uncovering the genomic consequences of a two-year life cycle. PLoS One. 2021; 16: e0255752. https://doi.org/10.1371/journal.pone.0255752 PMID: 34919547

94. Christensen KA, Leong JS, Sakhrani D, Biagi CA, Minkley DR, Withler RE, et al. Chinook salmon (Oncorhynchus tshawytscha) genome and transcriptome. PLOS ONE. 2018; 13: e0195461. https://doi.org/10.1371/journal.pone.0195461 PMID: 29621340

95. Korneliussen TS, Albrechtsen A, Nielsen R. ANGSD: Analysis of Next Generation Sequencing Data. BMC Bioinformatics. 2014; 15: 356. https://doi.org/10.1186/s12859-014-0356-4 PMID: 25420514

96. Goudet J. hierfstat, a package for r to compute and test hierarchical F-statistics. Molecular Ecology Notes. 2005; 5: 184–186. https://doi.org/10.1111/j.1471-8286.2004.00828.x

97. Nei M. Molecular Evolutionary Genetics. Molecular Evolutionary Genetics. Columbia University Press; 2019. https://doi.org/10.7312/nei-92038

98. Pante E, Simon-Bouhet B. marmap: A Package for Importing, Plotting and Analyzing Bathymetric and Topographic Data in R. PLOS ONE. 2013; 8: e73051. https://doi.org/10.1371/journal.pone.0073051 PMID: 24019892

99. Zhang C, Dong S-S, Xu J-Y, He W-M, Yang T-L. PopLDdecay: a fast and effective tool for linkage disequilibrium decay analysis based on variant call format files. Bioinformatics. 2019; 35: 1786–1788. https://doi.org/10.1093/bioinformatics/bty875 PMID: 30321304

100. Wickham H. ggplot2: Elegant Graphics for Data Analysis. New York: Springer-Verlag; 2009. Available: https://www.springer.com/gp/book/9780387981413.

101. Gutenkunst RN, Hernandez RD, Williamson SH, Bustamante CD. Inferring the Joint Demographic History of Multiple Populations from Multidimensional SNP Frequency Data. PLOS Genetics. 2009; 5: e1000695. https://doi.org/10.1371/journal.pgen.1000695 PMID: 19851460

102. Weir BS, Cockerham CC. Estimating F-Statistics for the Analysis of Population Structure. Evolution. 1984; 38: 1358–1370. https://doi.org/10.1111/j.1558-5646.1984.tb05657.x PMID: 28563791

103. Danecek P, Auton A, Abecasis G, Albers CA, Banks E, DePristo MA, et al. The variant call format and VCFtools. Bioinformatics. 2011; 27: 2156–2158. https://doi.org/10.1093/bioinformatics/btr330 PMID: 21653522

104. Paradis E, Schliep K. ape 5.0: an environment for modern phylogenetics and evolutionary analyses in R. Bioinformatics. 2019; 35: 526–528. https://doi.org/10.1093/bioinformatics/bty633 PMID: 30016406

105. Revell L. phytools: An R package for phylogenetic comparative biology (and other things). Methods in Ecology and Evolution. 2012; 3: 217–223. https://doi.org/10.1111/j.2041-210X.2011.00169.x

106. Jombart T, Balloux F, Dray S. adephylo: new tools for investigating the phylogenetic signal in biological traits. Bioinformatics. 2010; 26: 1907–1909. https://doi.org/10.1093/bioinformatics/btq292 PMID: 20525823

107. Delaneau O, Zagury J-F, Robinson MR, Marchini JL, Dermitzakis ET. Accurate, scalable and integrative haplotype estimation. Nat Commun. 2019; 10: 5436. https://doi.org/10.1038/s41467-019-13225-y PMID: 31780650

108. McVean G, Awadalla P, Fearnhead P. A Coalescent-Based Method for Detecting and Estimating Recombination From Gene Sequences. Genetics. 2002; 160: 1231–1241. https://doi.org/10.1093/genetics/160.3.1231 PMID: 11901136

109. Choi Y, Sims GE, Murphy S, Miller JR, Chan AP. Predicting the functional effect of amino acid substitutions and indels. PLoS ONE. 2012; 7: e46688. https://doi.org/10.1371/journal.pone.0046688 PMID: 23056405

110. Eyre-Walker A, Keightley PD. Estimating the Rate of Adaptive Molecular Evolution in the Presence of Slightly Deleterious Mutations and Population Size Change. Molecular Biology and Evolution. 2009; 26: 2097–2108. https://doi.org/10.1093/molbev/msp119 PMID: 19535738

111. Guéguen L, Gaillard S, Boussau B, Gouy M, Groussin M, Rochette NC, et al. Bio++: Efficient Extensible Libraries and Tools for Computational Molecular Evolution. Molecular Biology and Evolution. 2013; 30: 1745–1750. https://doi.org/10.1093/molbev/mst097 PMID: 23699471

112. Tarailo-Graovac M, Chen N. Using RepeatMasker to identify repetitive elements in genomic sequences. Curr Protoc Bioinformatics. 2009;Chapter 4: Unit 4.10. https://doi.org/10.1002/0471250953.bi0410s25 PMID: 19274634